From mesoscopic to macroscopic computations of dynamic contact lines

Shahriar Afkhami

Department of Mathematical Sciences
New Jersey Institute of Technology

IPAM: OILWS1: Multiphysics, Multiscale, and Coupled Problems in Subsurface Physics

Droplets in microchannels: Pore scale simulations

viscosity ratio $= \mu_d/\mu_e = 0.01$

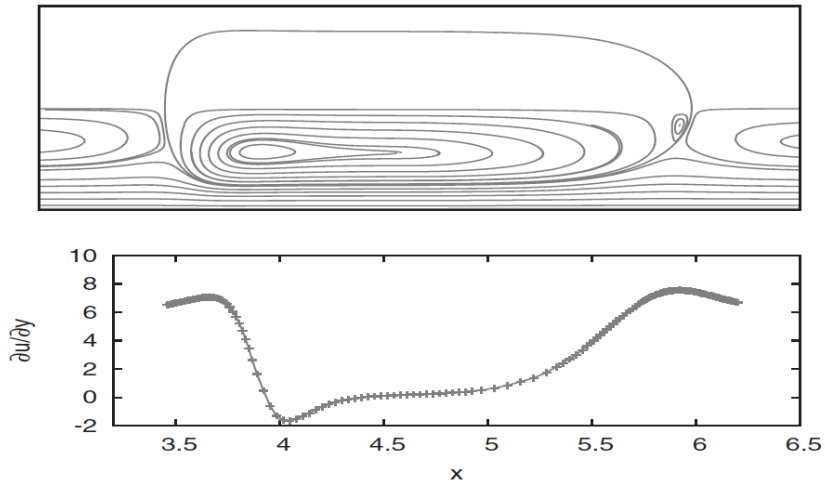

$\mathrm{Ca} = \mu_e \bar{U}/\gamma = 0.3$

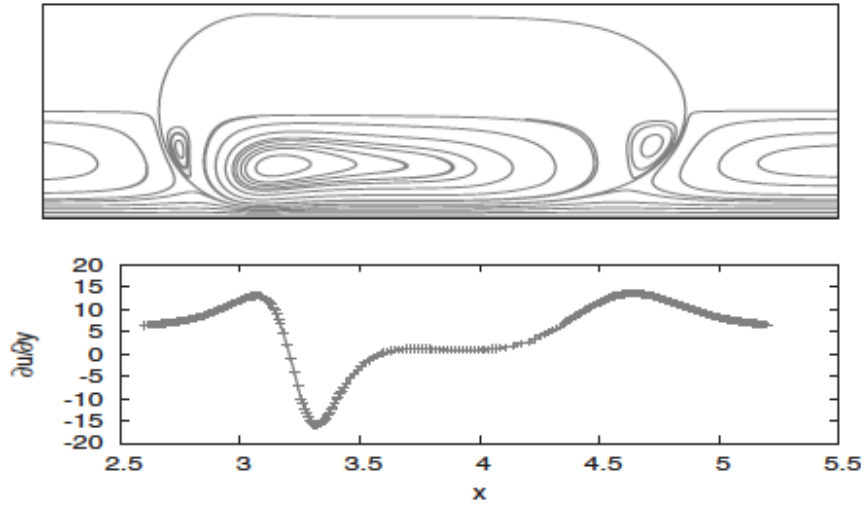

$\mathrm{Ca} = 0.04$

$h \propto \mathrm{Ca}^{2/3}$ [Bretherton, JFM 1961]

Afkhami et al., Phys. Fluids, 2011

Droplets in microchannels

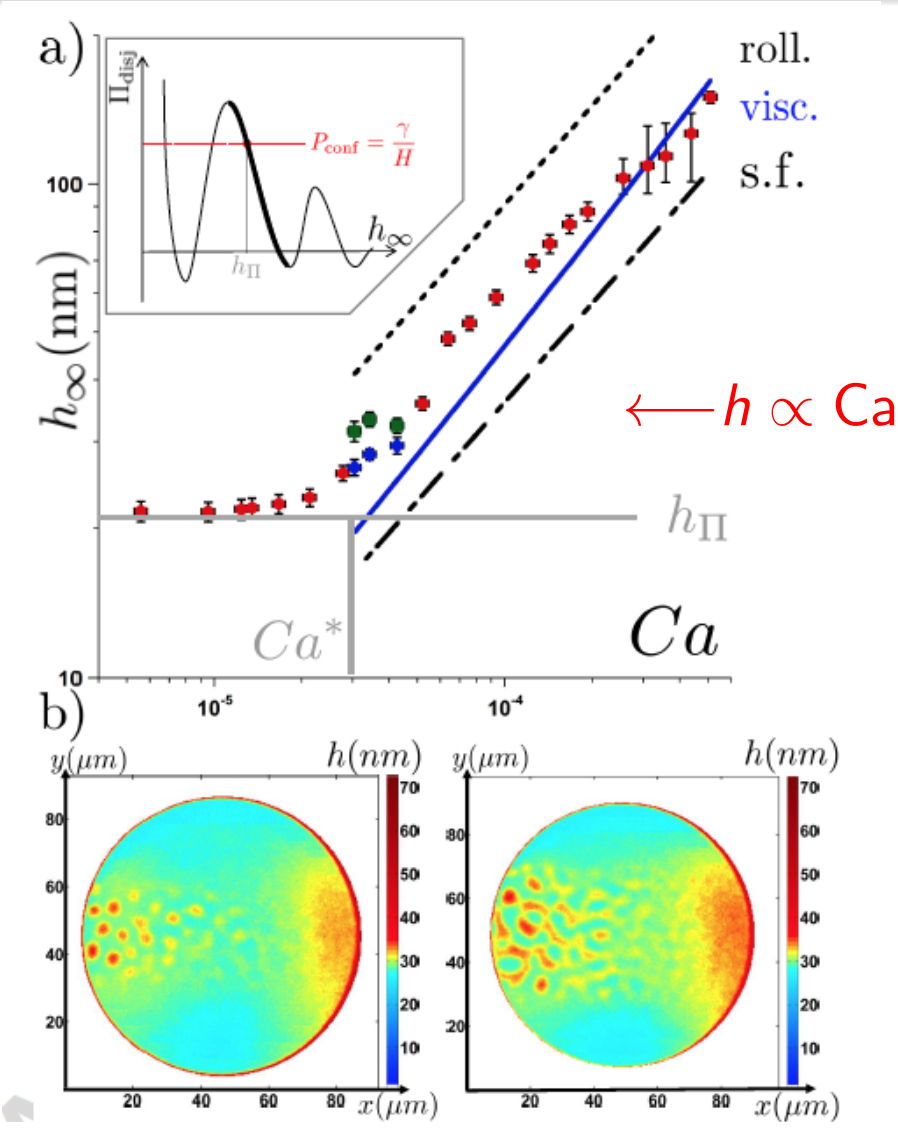

$\longleftarrow h \propto Ca^{2/3}$

Huerre et al., Phys. Rev. Lett., 2015

Modeling of thin films: breakup due to van der Waals force

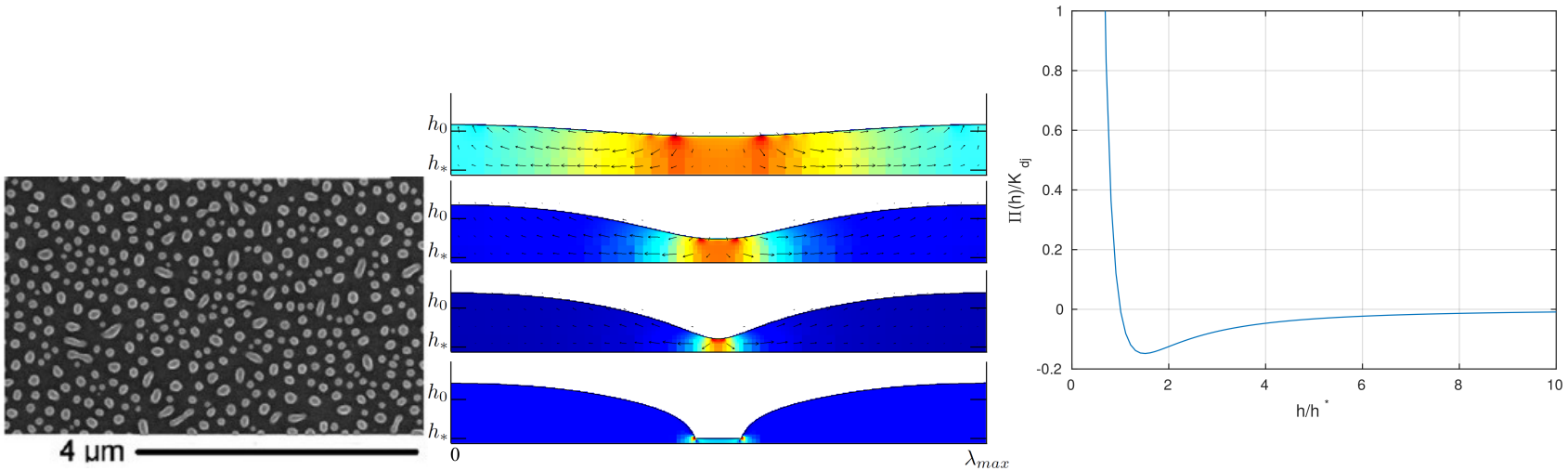

Break up of a perturbed thin film, $\lambda_{max} = 2\pi/k_{max}$

Dispersion relation of linearized equation with wavenumber k and growth rate ω:

$$\mu\omega/\gamma = -\frac{h_o^3}{3}\left[k^4 + k^2\Pi'(h_o)\right]$$

$$\Pi'(h_o) = \mathcal{K}_{dj}\left[m\left(\frac{h^*}{h_0}\right)^m - n\left(\frac{h^*}{h_0}\right)^n\right],\ \mathcal{K}_{dj} = \frac{\gamma(\cos\theta_{eq}-1)}{h^*}\frac{(m-1)(n-1)}{(m-n)}$$

Contact line phenomena in complex flows

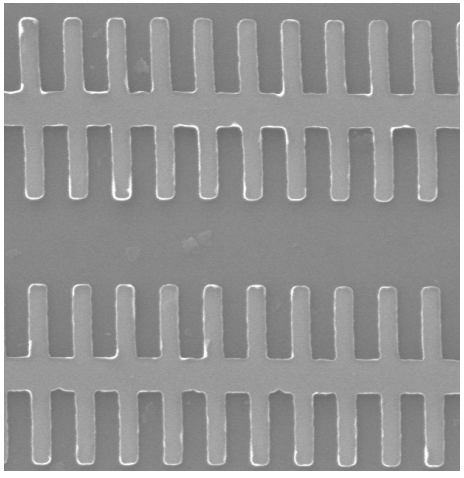

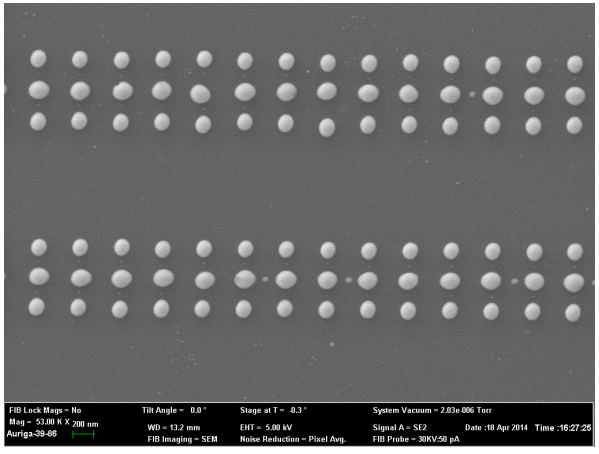

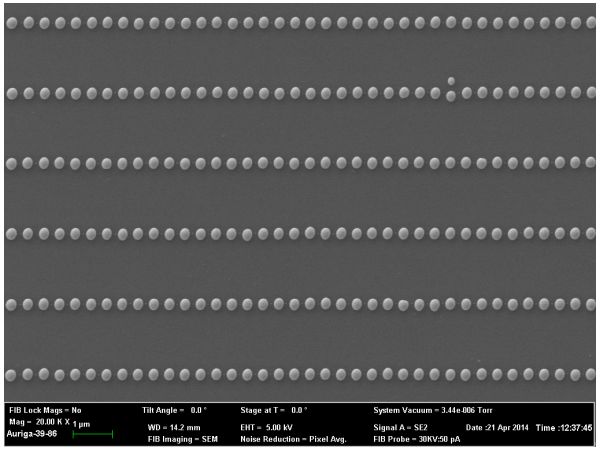

▸ Square-Wave-Simulations

Mahady et al., Phys. Fluids, 2015

Fluid motion in terms of fluxes

The motion of fluid is described by the conservation of mass:

$$\int_V \frac{\partial}{\partial t}\rho dV = -\int_V (\nabla \cdot \rho \mathbf{u}) dV$$

momentum:

$$\int_V \frac{\partial}{\partial t}\rho \mathbf{u} dV = -\int_V (\nabla \cdot \rho \mathbf{u}\mathbf{u}) dV + \int_V (\nabla \cdot \tilde{\tau}) dV + \int_V \mathbf{F} dV$$

energy:

$$\int_V \frac{\partial}{\partial t}\rho E dV = -\int_V (\nabla \cdot \rho \mathbf{u} E) dV - \int_V (\nabla \cdot q) dV$$

These equations are valid for any fluid.

$$\frac{\partial}{\partial t}\rho = -(\nabla \cdot \rho \mathbf{u})$$

$$\frac{\partial}{\partial t}\rho \mathbf{u} = -(\nabla \cdot \rho \mathbf{u}\mathbf{u}) + (\nabla \cdot \tilde{\tau}) + \mathbf{F}$$

$$\frac{\partial}{\partial t}\rho E = -(\nabla \cdot \rho \mathbf{u} E) - (\nabla \cdot q), \quad \nabla \cdot q = -k \nabla T$$

Methods for the Simulation of Free Surface Flows

- Free surface flows present several difficulties for numerical simulation
  - The governing equations (Navier-Stokes) do not explicitly include the interface: it's a moving boundary problem.
  - The topology of the interface may vary, as liquids break up and recoalesce.
  - The conditions on the surface - namely the surface tension - vary with the curvature. It is necessary not only to track the surface, but to be able to compute derivatives accurately.

Methods for the Simulation of Free Surface Flows

- Free surface flows present several difficulties for numerical simulation
  - The governing equations (Navier-Stokes) do not explicitly include the interface: it's a moving boundary problem.
  - The topology of the interface may vary, as liquids break up and recoalesce.
  - The conditions on the surface - namely the surface tension - vary with the curvature. It is necessary not only to track the surface, but to be able to compute derivatives accurately.
- Lagrangian methods explicitly track the free surface. Requires re-meshing with each step.

Methods for the Simulation of Free Surface Flows

- Free surface flows present several difficulties for numerical simulation
  - The governing equations (Navier-Stokes) do not explicitly include the interface: it's a moving boundary problem.
  - The topology of the interface may vary, as liquids break up and recoalesce.
  - The conditions on the surface - namely the surface tension - vary with the curvature. It is necessary not only to track the surface, but to be able to compute derivatives accurately.
- Lagrangian methods explicitly track the free surface. Requires re-meshing with each step.

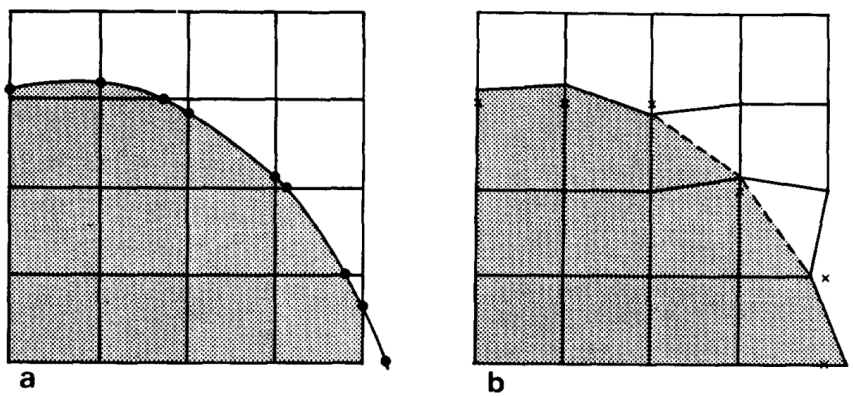

Moving mesh methods conform to shape of free surface.

Methods for the Simulation of Free Surface Flows

Front Tracking

- A numerical study of bubble interactions in Rayleigh-Taylor instability for compressible fluids,
  J. Glimm, X. Li, R. Menikoff, D. H. Sharp and Q. Zhang, Phys. Fluids, 1990.
- A front-tracking method for viscous, incompressible, multi-fluid flows,
  S. Unverdi and G. Tryggvason, J. Comput. Phys., 1992.

Level Set

- A level set approach for computing solutions to incompressible two-phase flow,
  M. Sussman, P. Smereka, and S. Osher, J. Comput. Phys., 1994.
- An adaptive level set approach for incompressible two-phase flows
  M. Sussman, A. Almgren, J. Bell, P. Colella, L. Howell, and M. Welcome, J. Comput. Phys., 1999.
- Level set methods: an overview and some recent results,
  S. Osher and R. Fedkiw, J. Comput. Phys., 2001.

Volume of Fluid

- Direct numerical simulation of free-surface and interfacial flow,
  R. Scardovelli, S. Zaleski, Ann. Rev. Fluid Mech., 1999.
- PROST: a parabolic reconstruction of surface tension for the volume-of-fluid method,
  Y. Renardy, M. Renardy, J. Comput. Phys., 2002.
- An accurate adaptive solver for surface-tension-driven interfacial flows,
  S. Popinet J. Comput. Phys., 2009.

Phase Field

- A diffuse-interface method for simulating two-phase flows of complex fluids,
  P. Yue, J. Feng, C. Liu, and J. Shen, J. Fluid Mech., 2004.
- A diffuse-interface method for simulating two-phase flows with soluble surfactants,
  K. Teigen, P. Song, J. Lowengrub, A. Voigt, J. Compt. Phys., 2011.

Two-Phase flows: Newtonian, incompressible, isothermal

$$T, \rho, \mu = \text{constant}$$

$$\nabla \cdot \mathbf{u} = 0$$

$$\rho(\frac{\partial \mathbf{u}}{\partial t} + (\nabla \cdot \mathbf{uu})) = \nabla \cdot \tilde{\tau} + \mathbf{F}$$

$$\tilde{\tau} = p\mathbf{I} + \mu\dot{\gamma}$$

$$\dot{\gamma} = \nabla \mathbf{u} + \nabla \mathbf{u}^T$$

$$\mathbf{F} = \gamma\kappa\delta_s\mathbf{n}$$

The volume of fluid method:

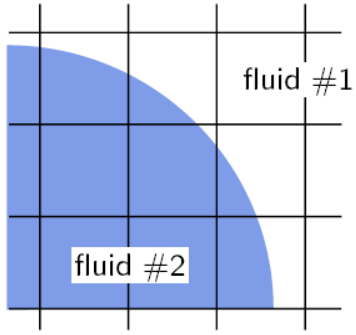

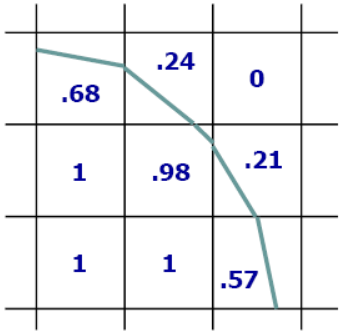

$$f_{i,j,k} = \frac{1}{\Omega_{i,j,k}} \int_{\Omega_{i,j,k}} f \, d\Omega$$

$$\frac{\partial f}{\partial t} + (\mathbf{u} \cdot \nabla) f = 0$$

$$\rho = \rho(f)$$

$$\mu = \mu(f)$$

S. Afkhami and M. Bussman, Int. J. Num. Meth. Fluids, 2007.
S. Afkhami et al., J. Comput. Phys., 2009

Research involving Volume-of-Fluid method:

- Viscoelastic two-phase flows (Renardy VT)
- Ferrofluid drops (Feng UBC)
- Variable surface tension flows (Stone Princeton) ▸ Simulation
- Nucleate boiling (Buongiorno MIT and Zaleski UPMC)

Contact angle

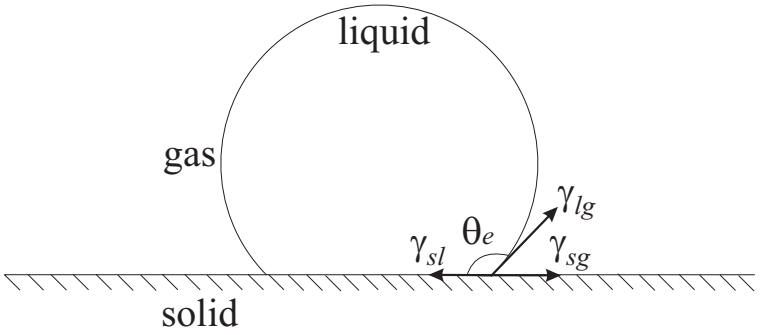

Equilibrium contact angle

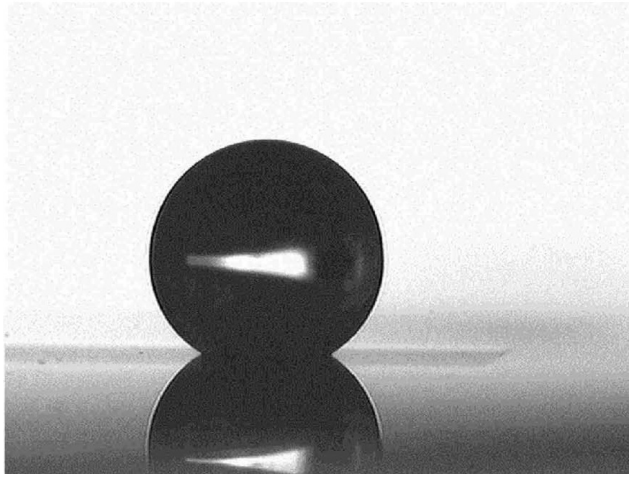

For a static contact line, Young's relation holds:

$$\gamma \cos\theta_e = \gamma_{sg} - \gamma_{sl}$$

Energy difference between wet and dry state - spreading parameter:

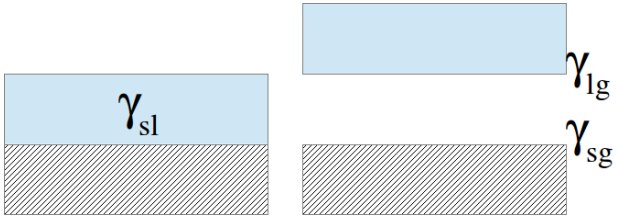

$$S_{eq} = \gamma_{sg} - (\gamma_{sl} + \gamma) = \gamma(\cos\theta_{eq} - 1)$$

Contact angle

[Ann. Rev. Fluid Mech., 45:269-292]

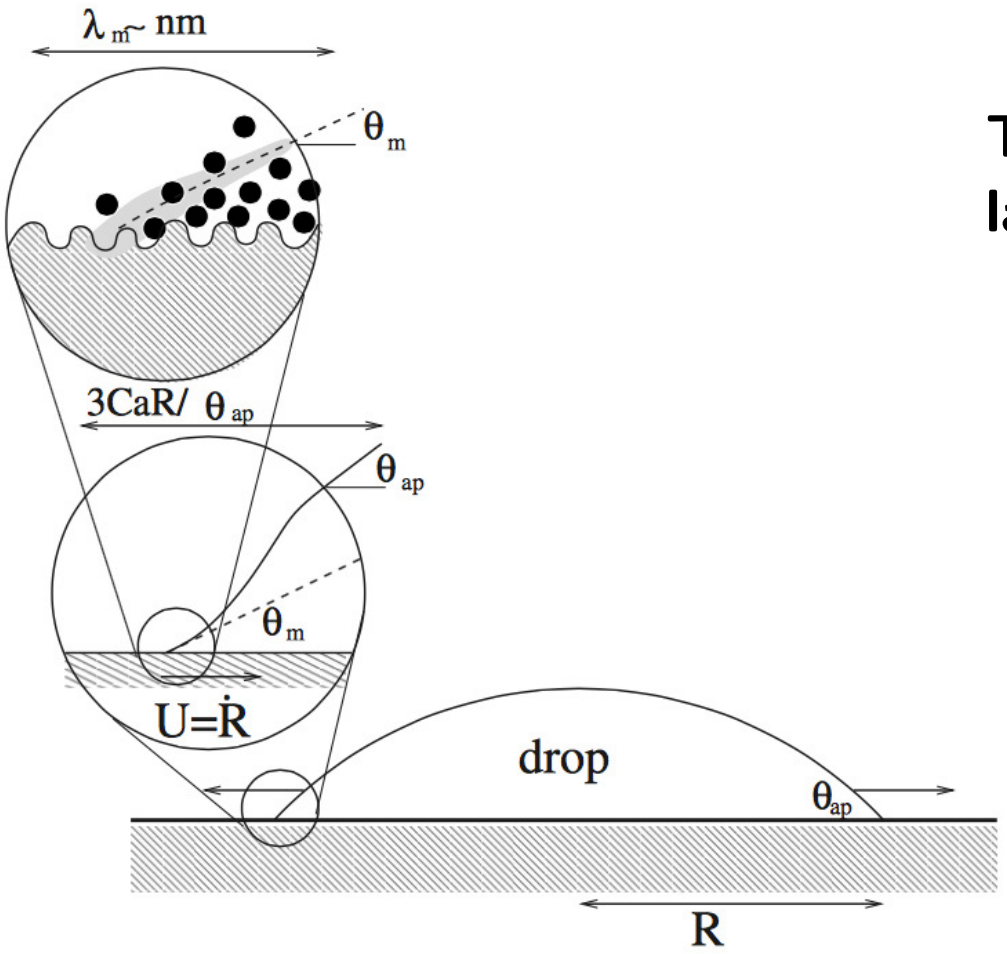

$$\theta_m = \cos^{-1}\left(\frac{\gamma_{sg}-\gamma_{sl}}{\gamma}\right)$$

There are two main challenges in large scale contact line modeling:

- to describe flow close to contact line
- to match hydrodynamic part of the problem to a microscopic neighborhood of contact line

Fluid/fluid/solid interactions

Potential (repulsive-attractive) on particle of phase i per unit volume of solid

$$\phi_i(r) = \rho_s \mathcal{K}_{is} \left(\left(\frac{\sigma_{is}}{r} \right)^p - \left(\frac{\sigma_{is}}{r} \right)^q \right)$$

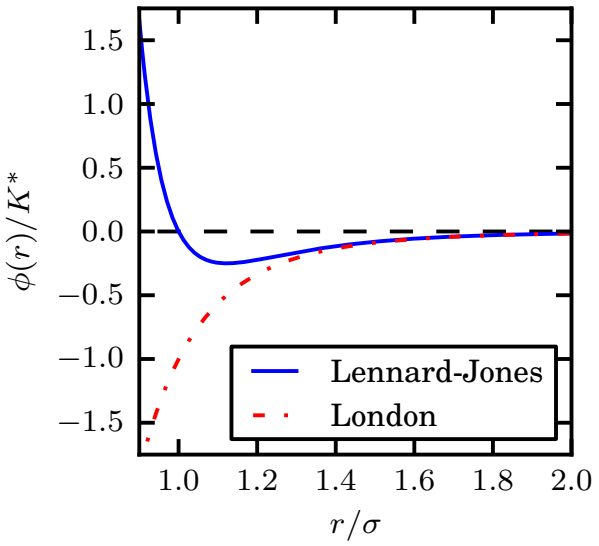

$(p, q) = (12, 6)$
$i =$ vapor,liquid
ρ_s : particles density in solid
σ_{is} : length scale determining minimum potential
$\mathcal{K}_{is}$: particle interaction strength
$r =$

$$\sqrt{(x_0 - x_s)^2 + (y_0 - y_s)^2 + (z_0 - z_s)^2}$$

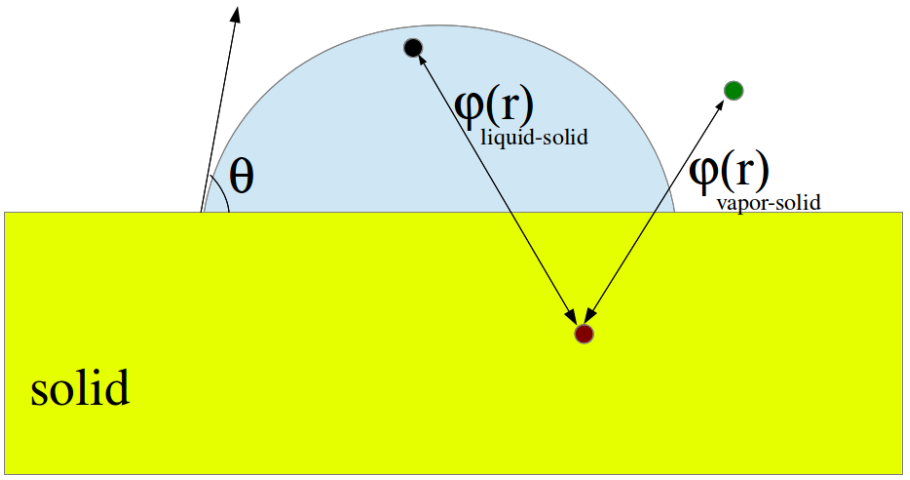

$$\phi_i(y) = \int_{-\infty}^{0} \int_{-\infty}^{\infty} \int_{-\infty}^{\infty} \phi_i(\mathbf{x}_0) dx_s dz_s dy_s$$

$$\phi_i(y) = \int_{-\infty}^{0}\int_{-\infty}^{\infty}\int_{-\infty}^{\infty}\phi_i(\mathbf{x}_0)dx_s dz_s dy_s =$$

$$2\pi\rho_s\mathcal{K}_{is}\sigma_{is}^3\left(\frac{1}{(p-2)(p-3)}\left(\frac{\sigma_{is}}{y}\right)^{p-3} - \frac{1}{(q-2)(q-3)}\left(\frac{\sigma_{is}}{y}\right)^{q-3}\right)$$

where y is the height of the particle above the solid substrate.

$$\phi_i(y) = K_{is}\left(\left(\frac{h_i^*}{y}\right)^m - \left(\frac{h_i^*}{y}\right)^n\right)$$

where $m = p-3$, $n = q-3$, and

$$h_i^* = \left(\frac{(q-2)(q-3)}{(p-2)(p-3)}\right)^{\frac{1}{p-q}}\sigma$$

$$K_{is} = 2\pi\rho_s\rho_l\mathcal{K}_{is}h_i^*\frac{((p-2)(p-3))^{\frac{q}{p-q}}}{((q-2)(q-3))^{\frac{p}{p-q}}}$$

Lennard-Jones and contact angles

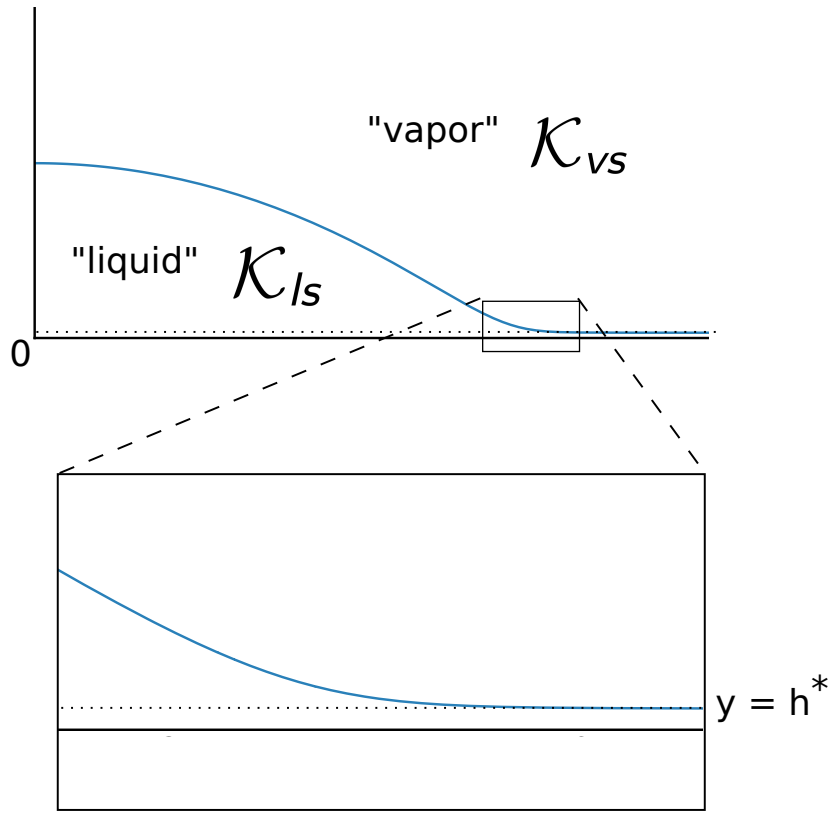

we refer to h^* as the precursor film thickness

Recall spreading parameter:

$$S_{eq} = \gamma_{sg} - (\gamma_{sl} + \gamma) = \gamma(\cos\theta_{eq} - 1)$$

Energy difference between wet and dry state:

$$\Delta E = \int_{\delta_0}^{\infty} (\phi_{vs} - \phi_{ls}) dy = S_{eq}$$

$$= (\mathcal{K}_{vs} - \mathcal{K}_{ls}) h^* \left[\frac{1}{m-1} \left(\frac{h^*}{\delta_0} \right)^{m-1} - \frac{1}{n-1} \left(\frac{h^*}{\delta_0} \right)^{n-1} \right]$$

Letting $\delta_0 = h^*$:

$$\mathcal{K}_{vs} - \mathcal{K}_{ls} = \frac{\gamma(1 - \cos\theta_{eq})}{h^*} \frac{(m-1)(n-1)}{(m-n)}$$

Volume-of-Fluid based Navier-Stokes solver

Method I: Body Force Formulation

$$\rho\left(\partial_t \mathbf{u} + \mathbf{u}\cdot\nabla\mathbf{u}\right) =$$

$$-\nabla p + \nabla\cdot\tilde{\tau} + \gamma\kappa\delta_s\mathbf{n} + \mathbf{F}_B(\mathbf{x})$$

$$\mathbf{F}_B(\mathbf{x}) = -\nabla(\phi_i(y))$$

$$\mathbf{F}_B(\mathbf{x}) = \left[f\mathcal{K}_{ls} + (1-f)\mathcal{K}_{vs}\right]\nabla(\phi_i(y))$$

Method II: Balanced Pressure Formulation

$$\rho\left(\partial_t \mathbf{u} + \mathbf{u}\cdot\nabla\mathbf{u}\right) =$$

$$-\nabla p^* + \nabla\cdot\tilde{\tau} + \gamma\left(\kappa - \frac{\mathcal{K}\phi_i(y)}{\gamma}\right)\delta_s\mathbf{n}$$

$$\mathcal{K} = \mathcal{K}_{ls} - \mathcal{K}_{vs}$$

$$p^* = p + \left[f\mathcal{K}_{ls} + (1-f)\mathcal{K}_{vs}\right]\left[-\phi_i(y)\right]$$

$$\phi_i(y) = \mathcal{K}_{is}\left[\left(\frac{h^*}{y}\right)^m - \left(\frac{h^*}{y}\right)^m\right]$$

The discrete approximation of $\mathbf{F}_B(\mathbf{x})$ and $\mathcal{K}\phi_i(y)$ are implemented in GERRIS (freely available at gfs.sf.net). [Mahady et al., JCP, 2015]

van der Waals Forces in VoF

Average - cell centered - force on cell $\mathcal{C}$ of size $\Delta_{\mathcal{C}}$

$$\mathbf{F}_B(\mathcal{C}) = \frac{1}{\Delta_{\mathcal{C}}^2}\int\int_{\mathcal{C}} \mathbf{F}_B(y)dxdy =$$

$$\frac{1}{\Delta_{\mathcal{C}}^2}\int\int_{\mathcal{C}} C(\mathbf{x})\mathbf{F}_l(y) + (1 - C(\mathbf{x}))\mathbf{F}_v(y)dxdy$$

where $C(\mathbf{x}) = 0, 1$ in vapor, liquid, is the color function. We replace $C(\mathbf{x})$ with its discrete approximation $f(\mathbf{x})$:

$$\mathbf{F}_B(\mathcal{C}) \sim \frac{1}{\Delta_{\mathcal{C}}^2}\int\int_{\mathcal{C}} f\mathbf{F}_l(y) + (1 - f)\mathbf{F}_v(y)dxdy$$

The problem then is the accurate approximation of this integral.

$$\mathbf{F}_B(\mathcal{C}) \sim f(\mathcal{C})\mathbf{F}_l(y(\mathcal{C})) + [1 - f(\mathcal{C})]\mathbf{F}_v(y(\mathcal{C}))$$

van der Waals Forces in VoF

$$\mathbf{F}_B(\mathcal{C}) \sim \frac{1}{\Delta_{\mathcal{C}}^2}\left(\int\int_{\mathcal{C}_l} \mathbf{F}_l(y)dxdy + \int\int_{\mathcal{C}_v} \mathbf{F}_v(y)dxdy\right)$$

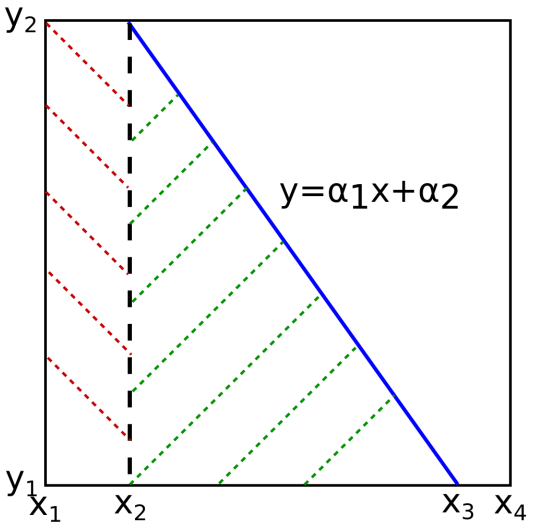

These integrals are computed analytically given knowledge of normal vector and an equation for reconstructed interface.

$$\int\int_{\mathcal{C}_l} \mathbf{F}_l(y)dxdy = \begin{cases} \int_{x_1}^{x_2}\int_{y_1}^{y_2} \mathbf{F}_l(y)dydx + \\ \int_{x_2}^{min\{x_3,x_4\}}\int_{y_1}^{\alpha_1 x+\alpha_2} \mathbf{F}_l(y)dydx & \text{if } x_2 > x_1 \\ \int_{x_1}^{min\{x_3,x_4\}}\int_{y_1}^{\alpha_1 x+\alpha_2} \mathbf{F}_l(y)dydx & \text{else} \end{cases}$$

Contact Angles, $\theta_i = \theta_{eq}$, $\gamma = \mu = \rho = 1$

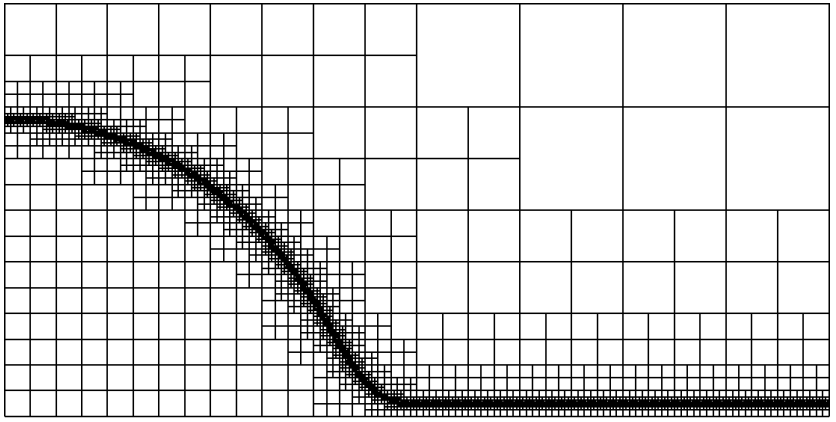

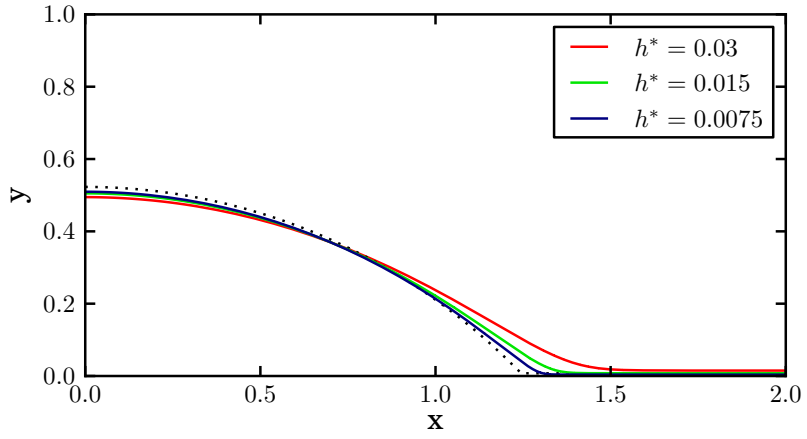

$\theta_{eq} = \pi/4$

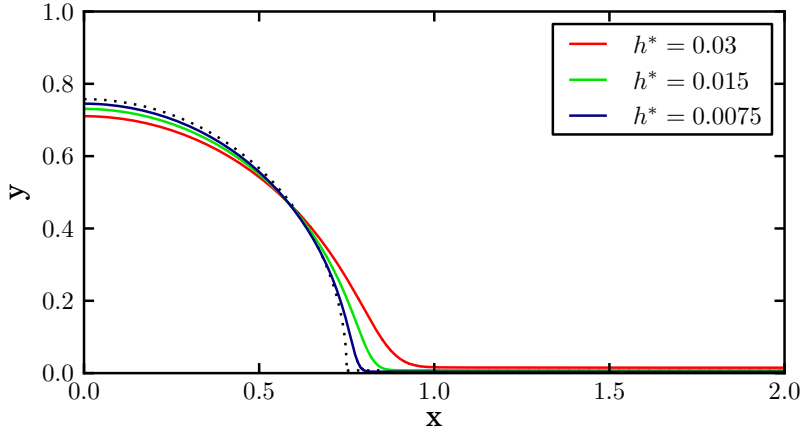

$\theta_{eq} = \pi/2$

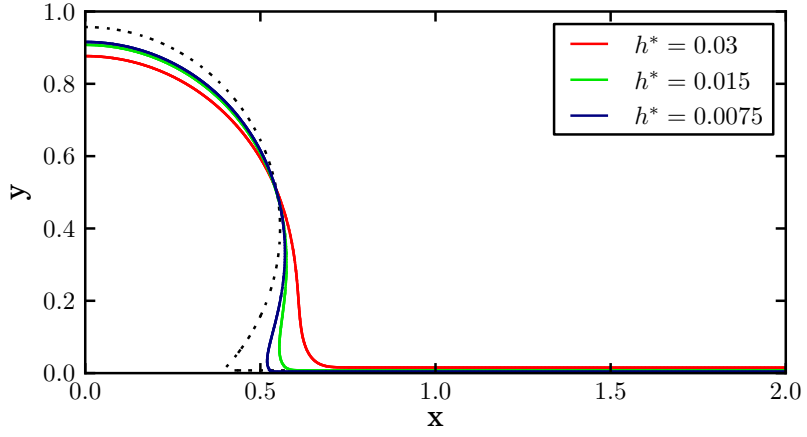

$\theta_{eq} = 3\pi/4$

Convergence Tests, $\theta_{eq} = \pi/2$

Δ	Reduced Pressure	Body Force
$1/2^5$	6.1×10^{-2}	7.0×10^{-3}
$1/2^6$	2.6×10^{-3}	4.3×10^{-3}
$1/2^7$	8.0×10^{-4}	3.8×10^{-4}

Comparison of the mesh convergence in profile shape.

h^*	Reduced Pressure	Body Force
0.03	1.3636	1.3783
0.015	1.4525	1.4702
0.0075	1.4939	1.5391

Comparison of the influence of h^* on θ_{num}.

Spreading: $\pi/2 = \theta_i \to \theta_{eq} = \pi/6$, $\gamma = \mu = \rho = 1$

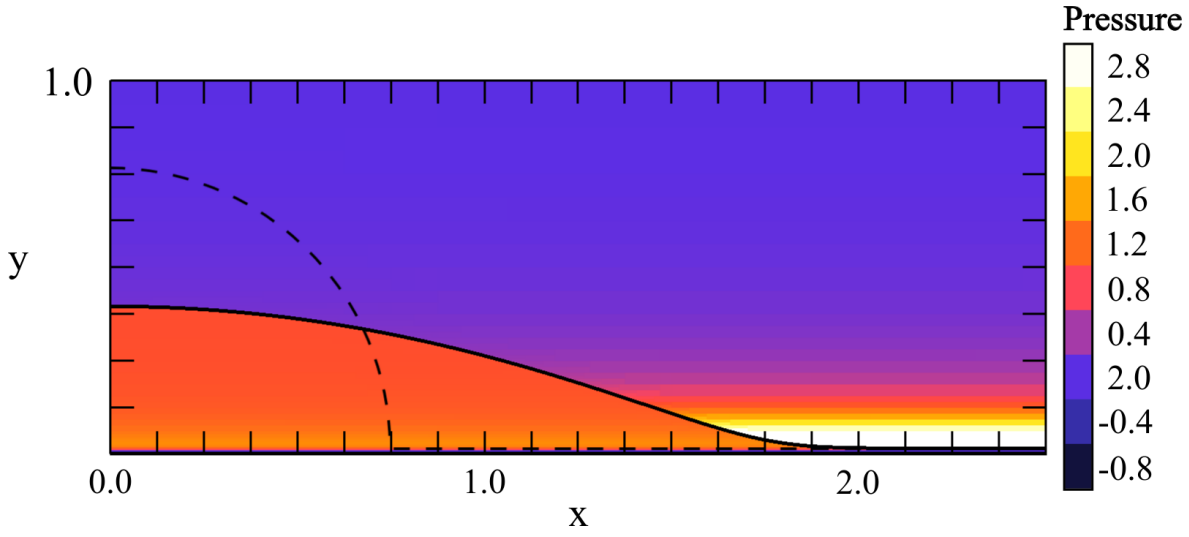

Cox-Voinov:

$$\theta^3 - \theta_{eq}^3 \propto v_f$$

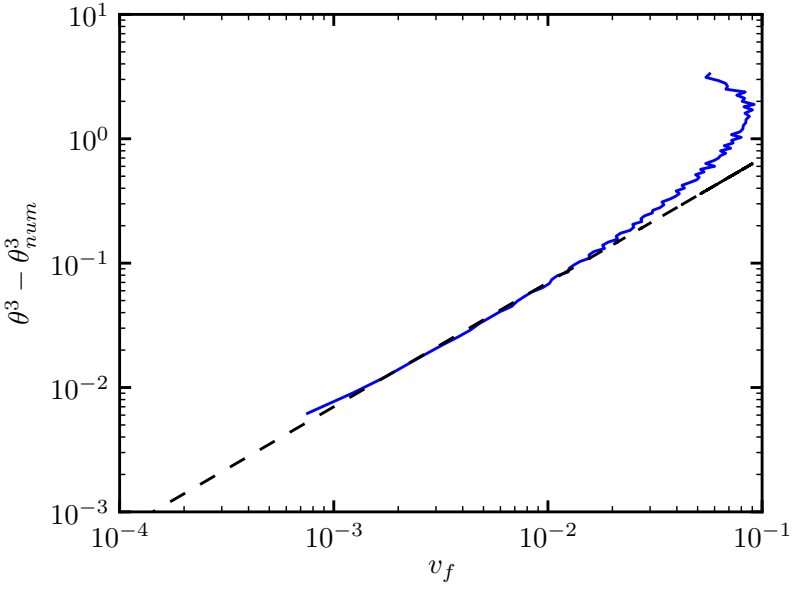

Film Rupture I: Dispersion Curves and Contact Angles, $\mathrm{Oh} = \mu/\sqrt{\gamma\rho L} = 0.45$ (liquid copper of 8nm thick)

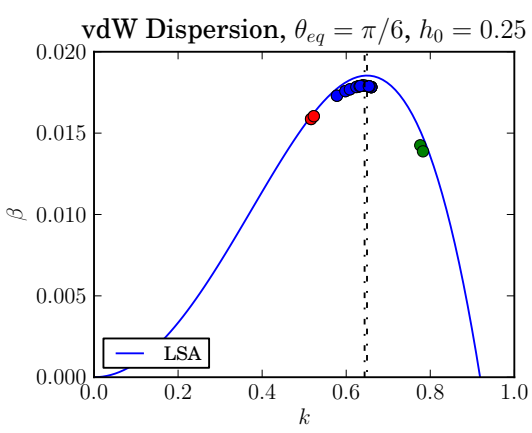

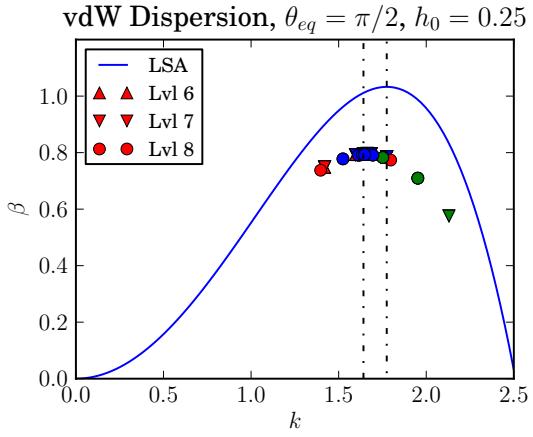

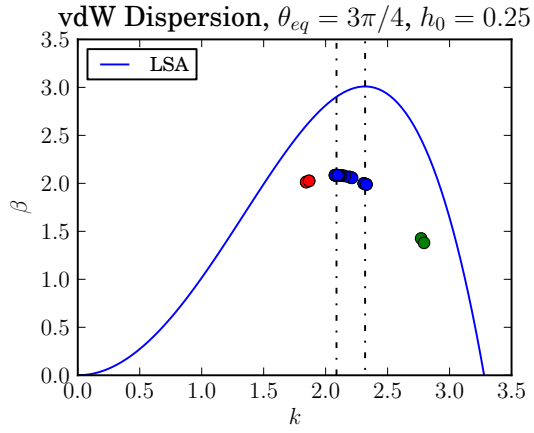

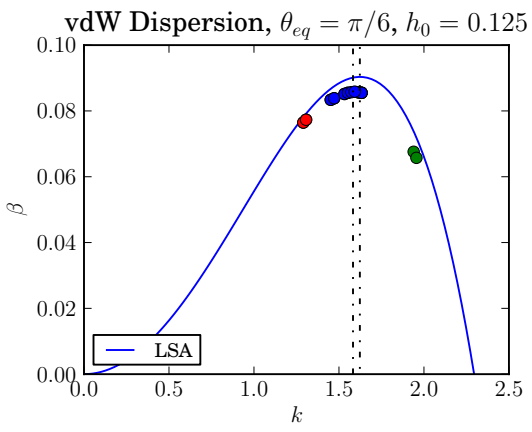

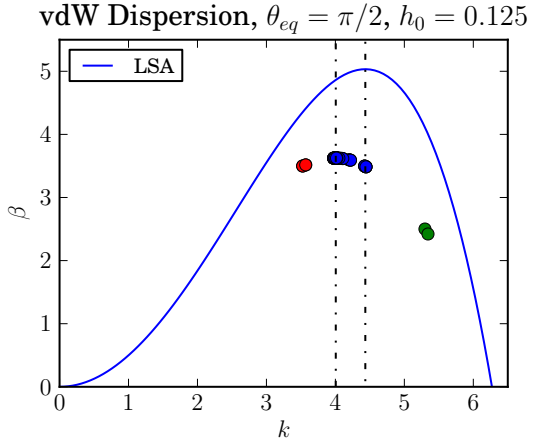

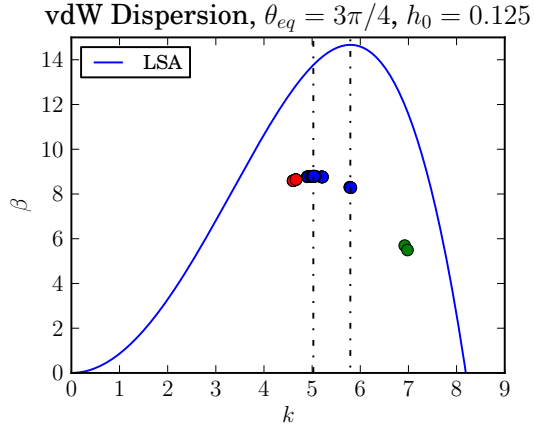

$$\beta = -\frac{h_o^3}{3}\left[k^4 + k^2\phi'(h_o)\right]$$

$$\phi'(h_o) = -\frac{\mathcal{K}}{\gamma h_0}\left[m\left(\frac{h^*}{h_0}\right)^m - n\left(\frac{h^*}{h_0}\right)^m\right],\ \mathcal{K} = \frac{\gamma(\cos\theta_{eq}-1)}{h^*}\frac{(m-1)(n-1)}{(m-n)}$$

Nonlinear film breakup: 2D results

$$h(x,0) = h_0 + \zeta(x), \text{ where } \zeta(x) = \sum_{i=1}^{60} \delta_i \cos\left(\frac{2\pi x}{\lambda_i}\right)$$

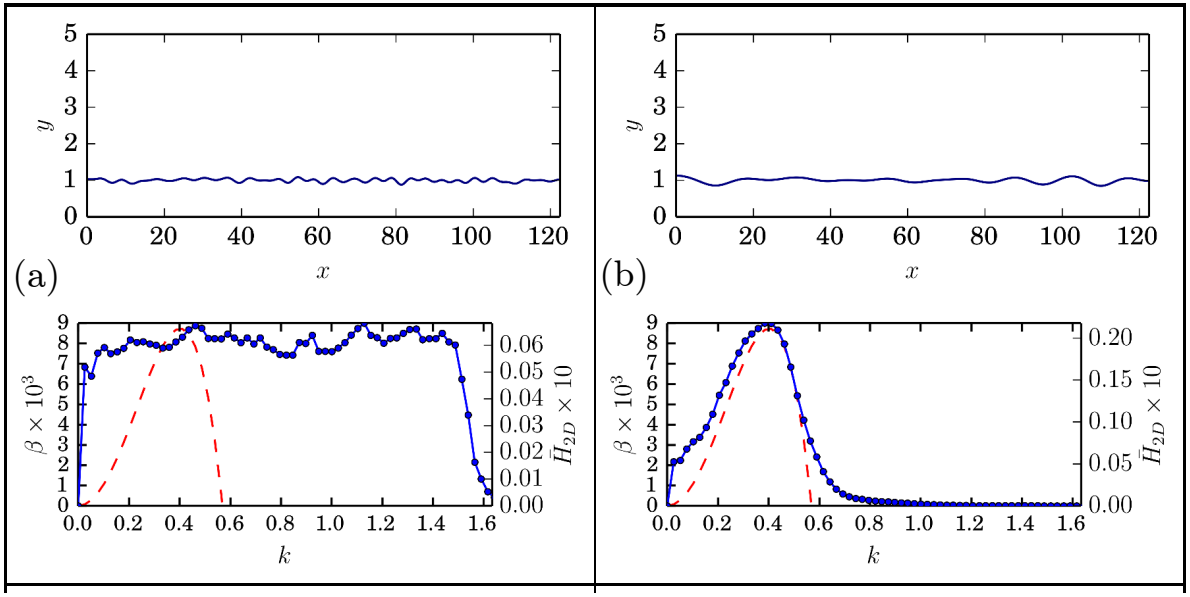

$$\bar{H}_{2D}(t,k) = \frac{1}{N_s} \sum_{j=1}^{N_s} \hat{H}_j(t,k).$$

Nonlinear film breakup: 2D results

- Simulation $\mathrm{Oh} = 0.0049$
- Simulation $\mathrm{Oh} = 0.049$
- Simulation $\mathrm{Oh} = 4.9$

Nonlinear film breakup: 2D results

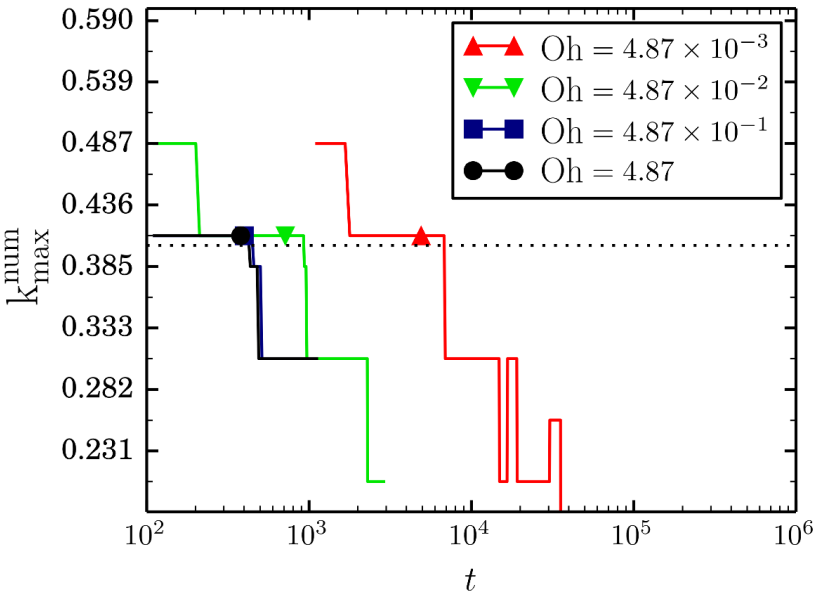

$\theta_{\mathrm{eq}} = 0.439\pi$

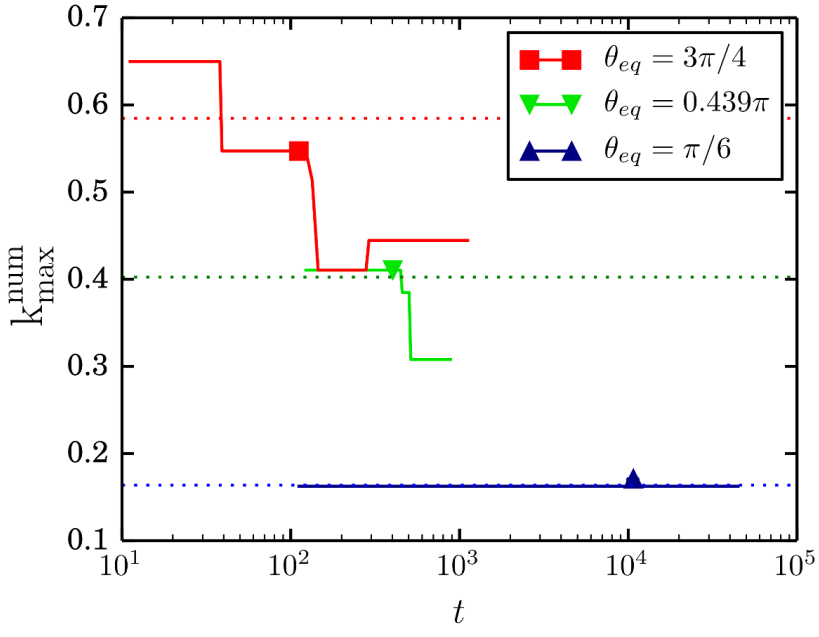

$\mathrm{Oh} = 0.487$

Nonlinear film breakup: 3D results

$$h(t=0,x,z) = h_0 + \zeta(x,z),$$
$$\zeta(x,y) = \sum_{i=1}^{30}\sum_{j=1}^{30} \delta_{ij} \cos\left(\frac{2\pi x}{\lambda_i}\right) \cos\left(\frac{2\pi z}{\lambda_j}\right),$$

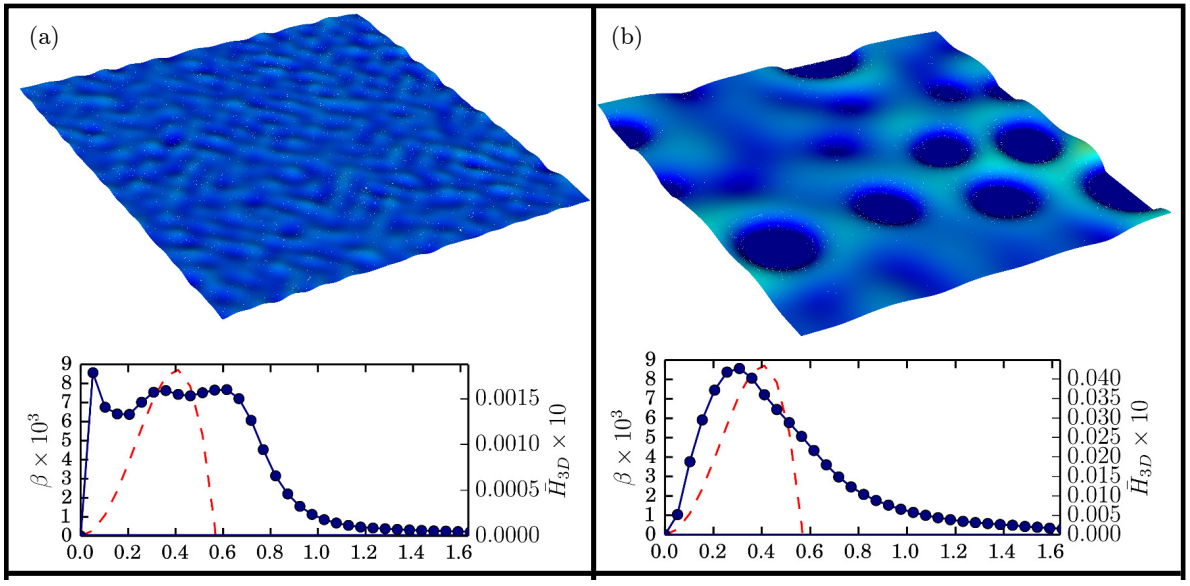

$$\bar{H}_{3D}(t,k) = \frac{1}{N_s}\sum_{j=1}^{N_s}\frac{1}{2}\left(\hat{H}_j(t,k,0) + \hat{H}_j(t,0,k)\right).$$

Spinodal dewetting: 3D results, liquid copper, $\theta_{eq} = 0.439\pi$, $\quad$ Oh $= 0.487$

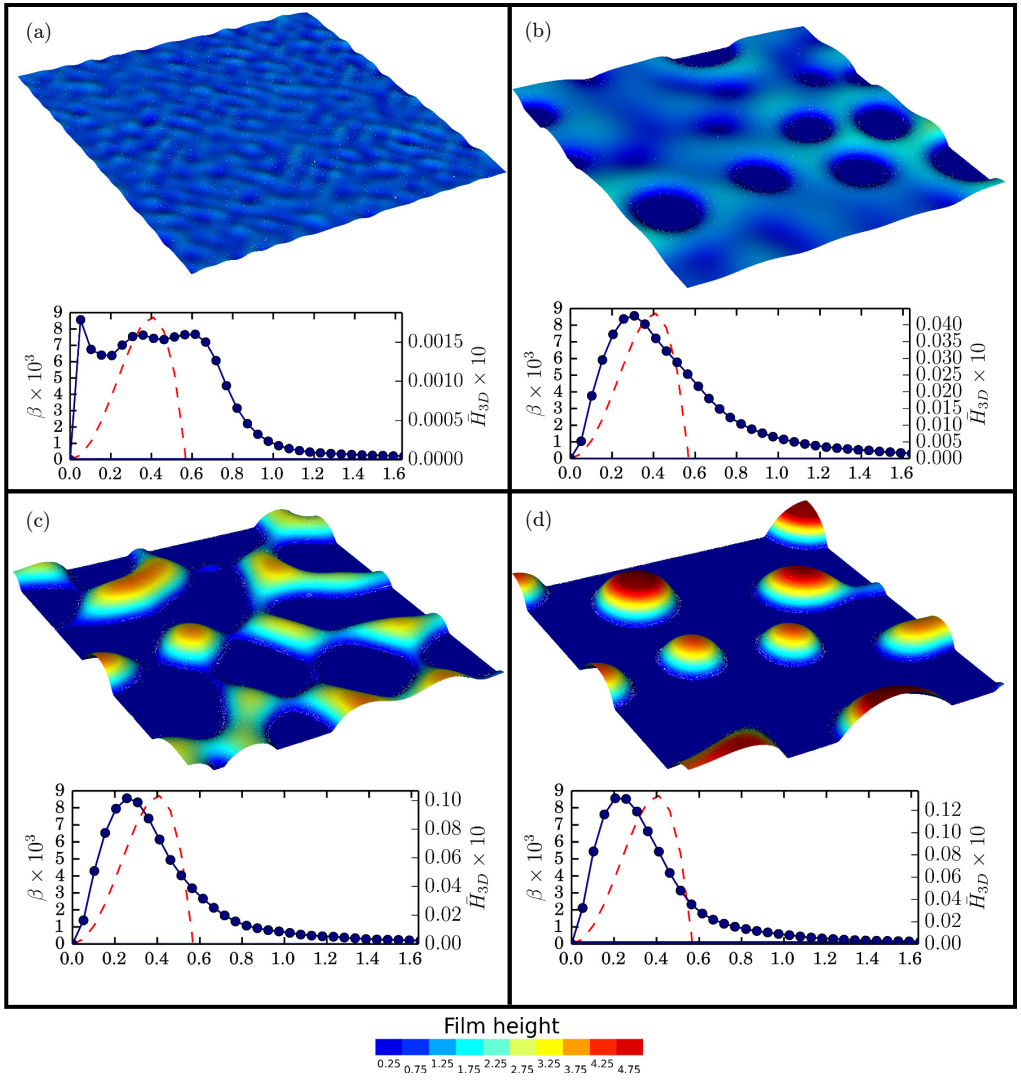

[Mahady et al., PoF, 2016]

Spinodal dewetting: 3D results, liquid copper, $\theta_{\text{eq}} = 0.439\pi, \quad \text{Oh} = 0.487$

▸ Simulation

$4nm$ thick

▸ Simulation

$8nm$ thick

Spinodal dewetting: 2D vs 3D results, $\mathrm{Oh} = \mu/\sqrt{\gamma\rho L} = 0.48$

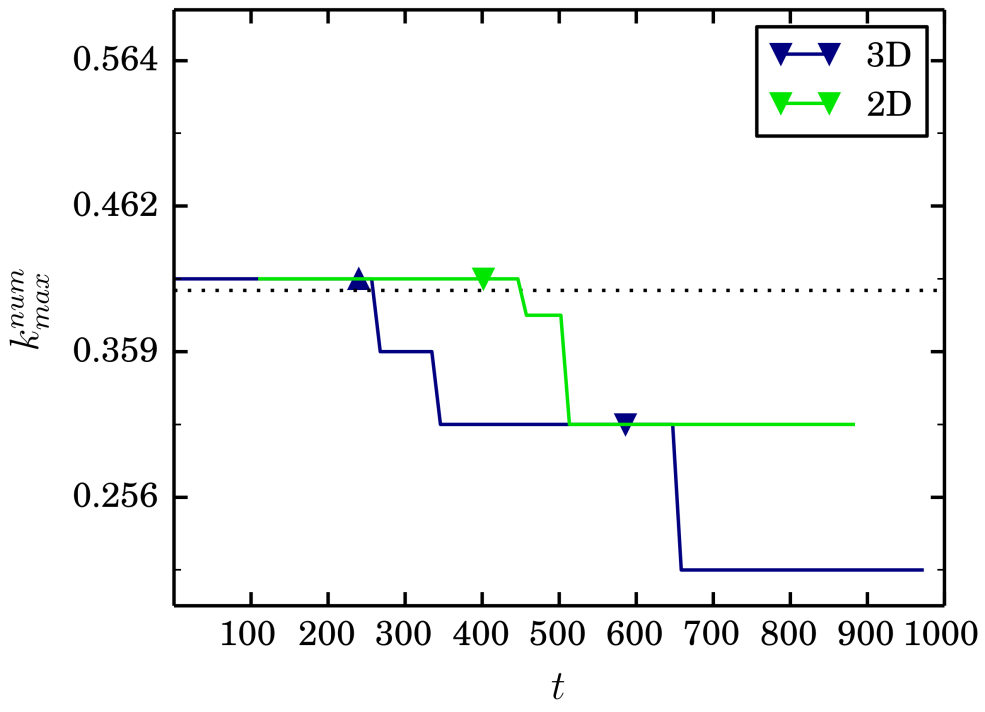

Conclusions

- Interaction between fluid phases and a substrate can be included in a robust manner.
- Very little additional computational cost is required ($O(N)$).
- Simulations of arbitrary, particularly large ($> \pi/2$), contact angles are possible.
- Film rupture agrees with LSA for small contact angles, but deviates for larger angles.
- Inertia plays a small role in the initial breakup pattern of films, but impacts the end spacing of drops through recoalescence.
- Film rupture in 3D agrees with previous experimental and theoretical works.

Acknowledgments
Kyle Mahady and Lou Kondic, NJIT
Stéphane Zaleski, Institut Jean Le Rond d'Alembert, Université Pierre et Marie Curie
NSF DMS-1320037 and NSF-CBET-1604351

Landau–Levich–Derjaguin film

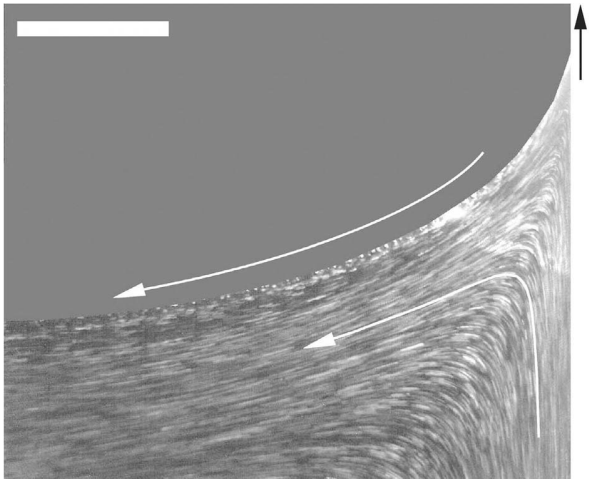

From Mayer and Krechetnikov [Phys. Fluids 24, (2012)]

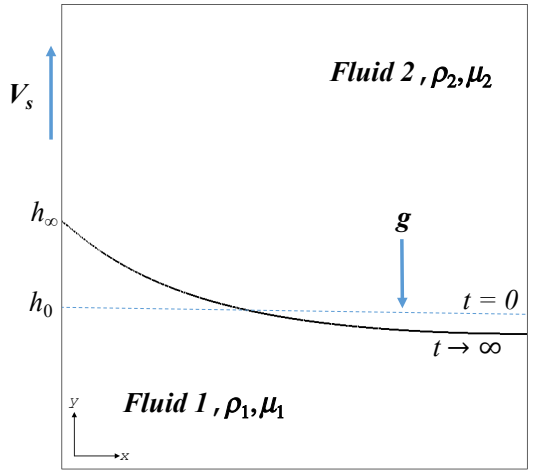

$$\mathrm{Ca} = \mu_1 V_s/\gamma$$

Low Ca:
Contact line equilibrates at a height

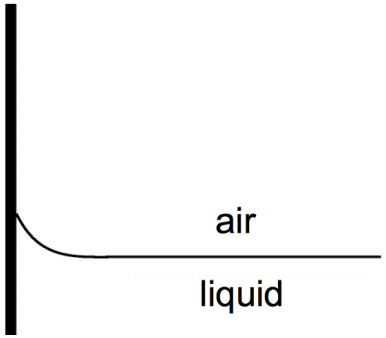

High Ca:
Meniscus transitions to a film

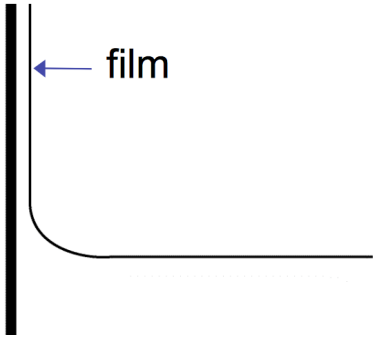

Can we numerically predict the transition?
Is this transition universal?

Modeling of thin films, $\theta_e \to 0$

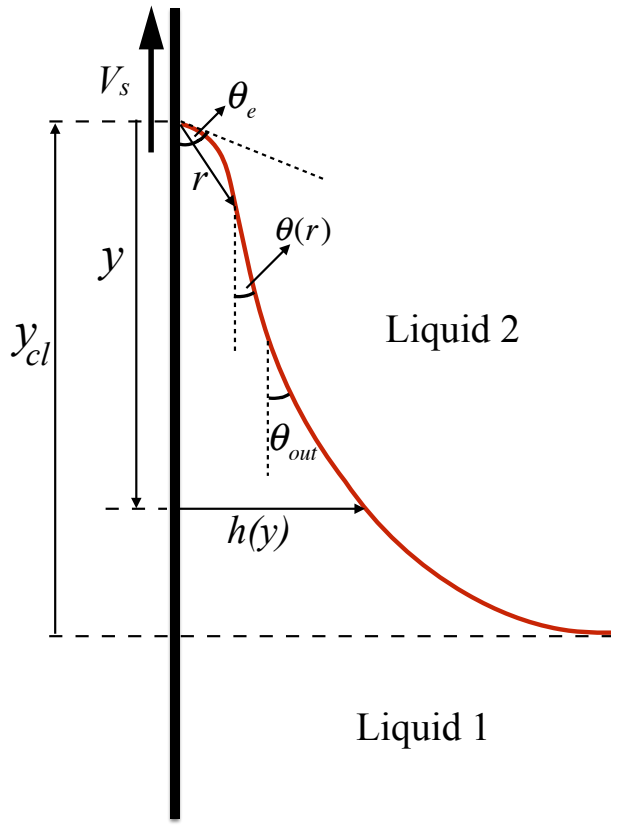

$$\frac{\partial^3 h}{\partial y^3} = \frac{3\mathrm{Ca}}{(h^2 + 3\lambda h)}$$

$\frac{\mathrm{Ca}}{(h^2+\lambda h)}$ corresponds to viscous forces that diverge as $h \to 0$.

$$0 = \nabla \cdot \tilde{\tau}_i, \quad \nabla \cdot \mathbf{u}_i = 0$$

$$\tilde{\tau}_i = -p\mathbf{I} + \mu_i(\nabla \mathbf{u}_i + \nabla \mathbf{u}_i^T), \quad i = 1, 2$$

at $x = h(y)$:

$$[\mathbf{u} \cdot \mathbf{n}] = [\mathbf{u} \cdot \mathbf{t}] = 0$$

$$[\mathbf{n} \cdot \tilde{\tau} \cdot \mathbf{n}] = -\gamma \nabla \cdot \mathbf{n}, \quad [\mathbf{n} \cdot \tilde{\tau} \cdot \mathbf{t}] = 0$$

at $x = 0$:

$$v - V_s = \lambda \frac{\partial v}{\partial x}, \quad u = 0$$

λ is slip length

kinematic boundary condition:

$$0 = -\frac{\partial}{\partial y} \int_0^{h(y)} v \, dx$$

Modeling of thin films, $\theta_e \to 0$

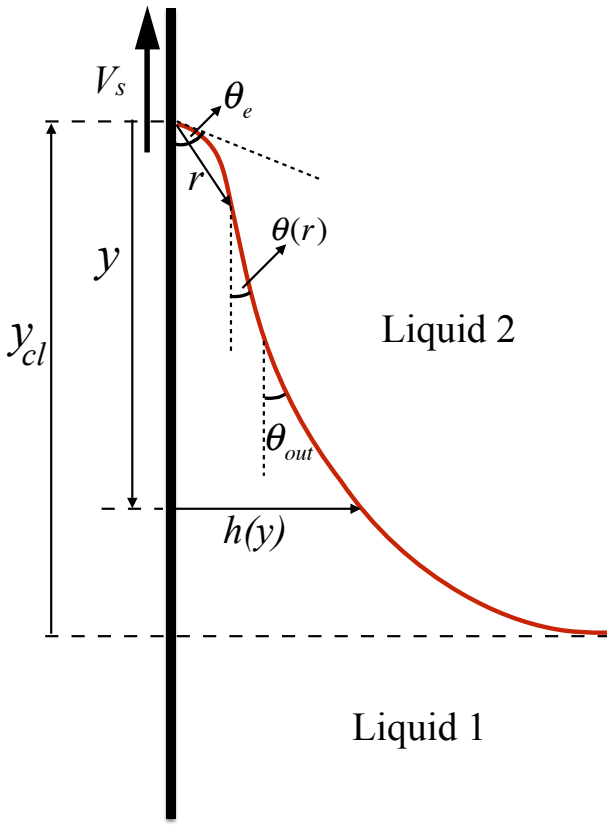

inner region: $\dfrac{\partial^3 h}{\partial y^3} = \dfrac{3\mathrm{Ca}}{(h^2 + 3\lambda h)}$

outer region: $\kappa = y_{cl} - y$

$l_c = \sqrt{\gamma/[(\rho_1 - \rho_2)g]}$
is the capillary length scale

$$\mathrm{Ca}_{cr} = (\theta_e^3/9)\left[\ln\left(\frac{[\mathrm{Ca}_{cr}]^{1/3}\theta_e}{18^{1/3}\pi[\mathrm{Ai}(S_{\max})]^2\sqrt{2}\lambda}\right)\right]^{-1}$$

$$\theta_{out} \to 0, \kappa = \sqrt{2}$$

[Chan, Snoeijer, Eggers, Phys. Fluids 24 (2012).]

Height-Function method: arbitrary contact angle

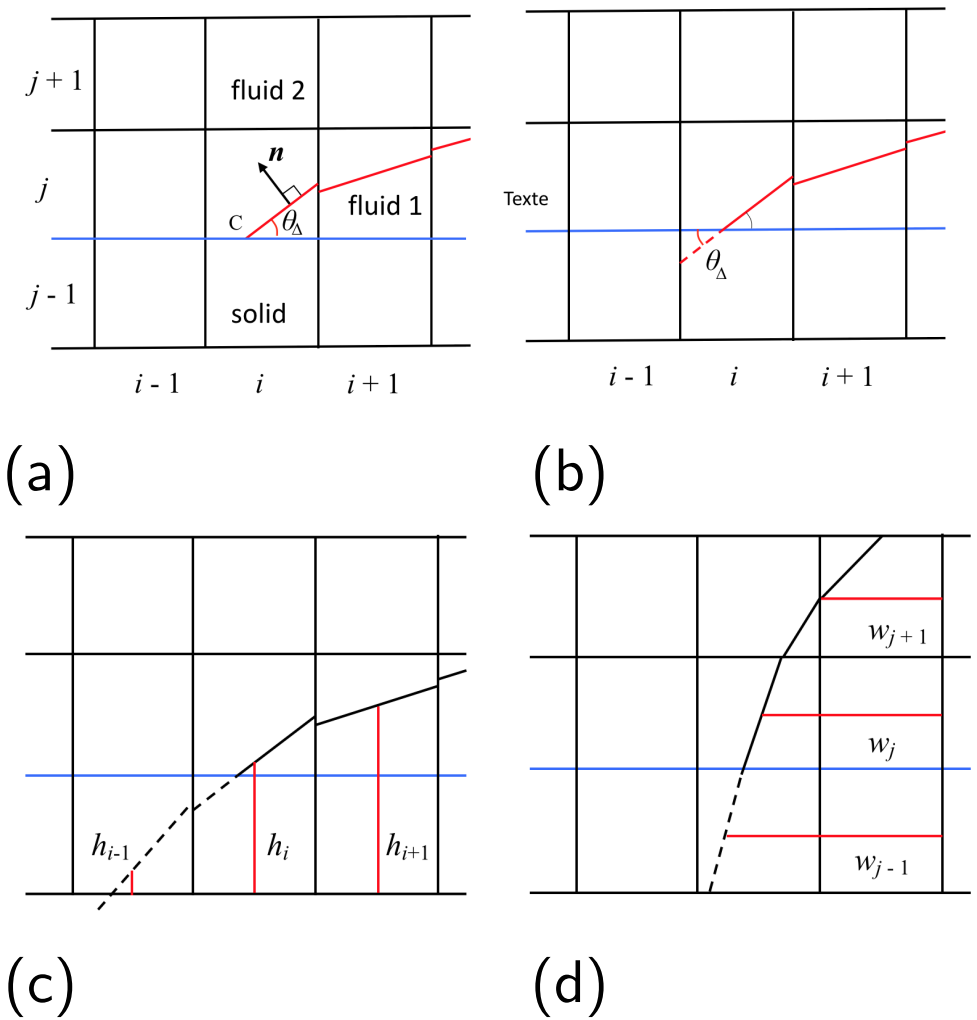

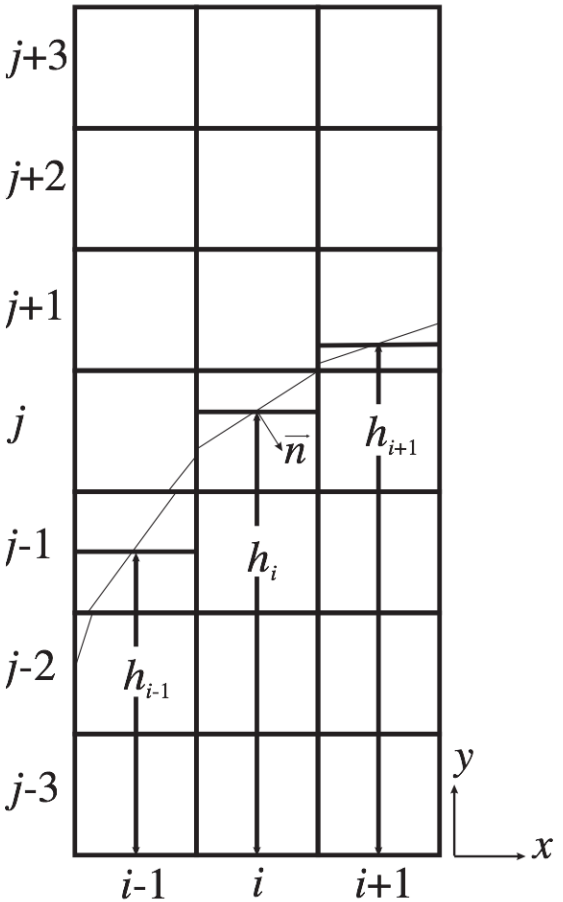

$$\kappa = \frac{h_{xx}}{(1 + h_x^2)^{3/2}}$$

$$\mathbf{n} = (h_x, -1)$$

S. Afkhami and M. Bussman, Int. J. Num. Meth. Fluids, 2007.
S. Afkhami et al., J. Comput. Phys., 2009

Numerical model

- an implicit (numerical) slip at the grid scale
- well-defined static contact angle
- gravity, surface tension, viscosity/density contrast

not included:

- dynamic angle model
- microscopic physics

Numerical setup

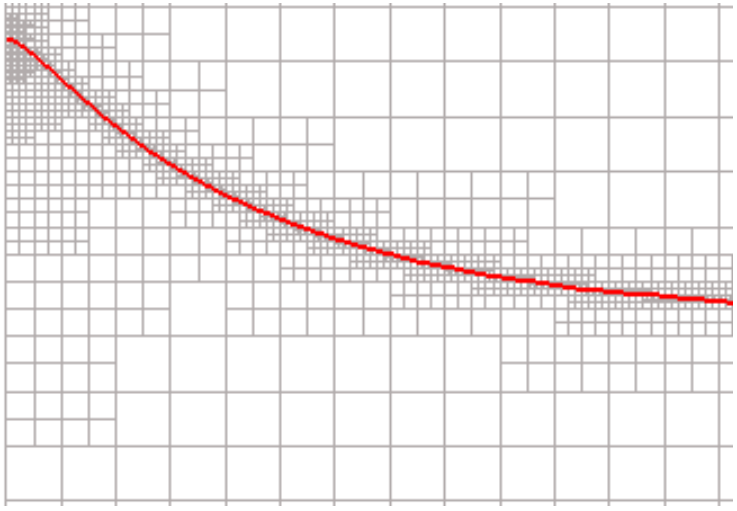

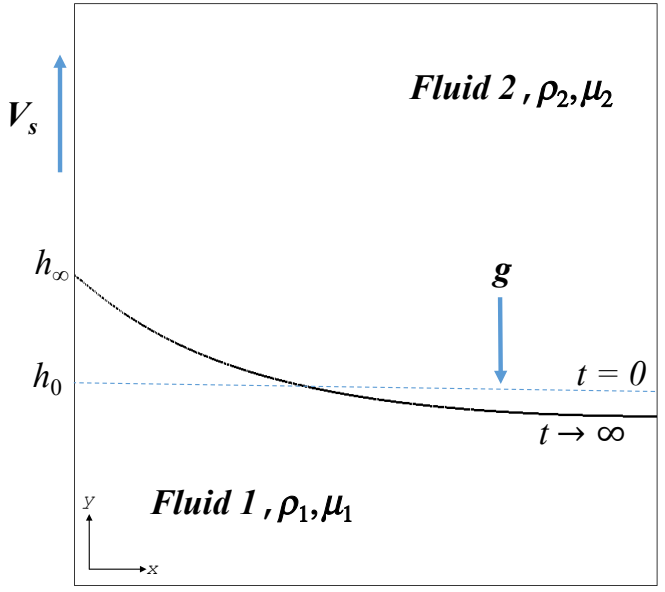

- $0.001 \leq \mathrm{Ca} = \mu_1 V_s/\gamma \leq 0.1$
- $20^\circ \leq \theta \leq 110^\circ$
- $l_c = \sqrt{\gamma/[(\rho_1 - \rho_2)g]} \approx L/10$
  capillary length of water/air ~ 2 mm
- $1/128 \leq l_c/\Delta \leq 1/32$

Numerical results: stationary meniscus

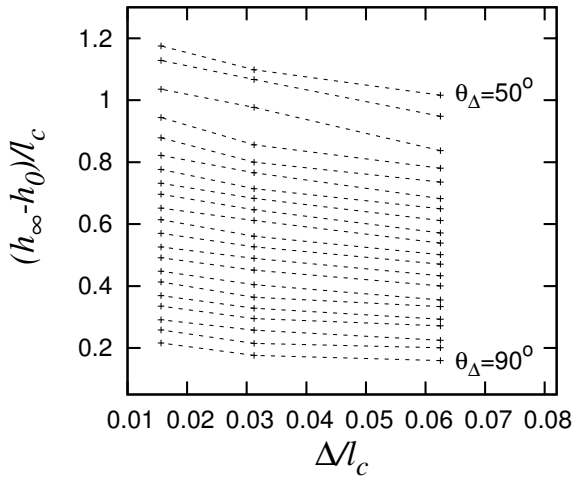

$\mathrm{Ca} = 0.01$

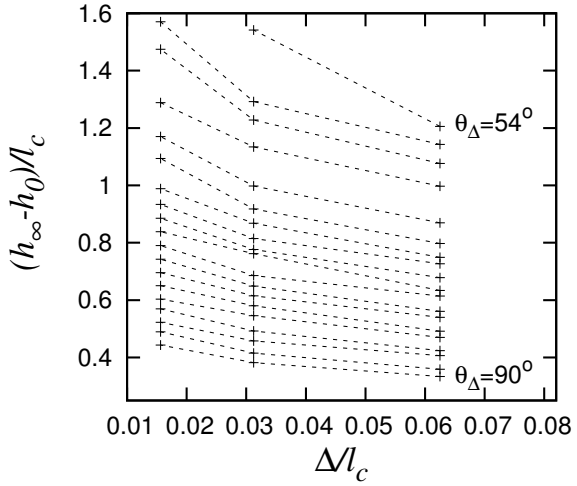

$\mathrm{Ca} = 0.02$

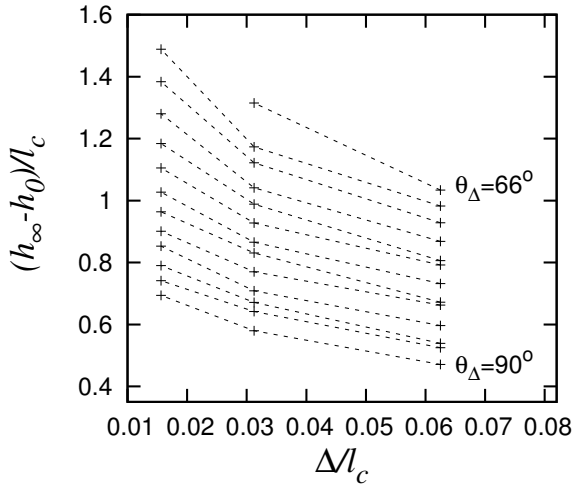

$\mathrm{Ca} = 0.03$

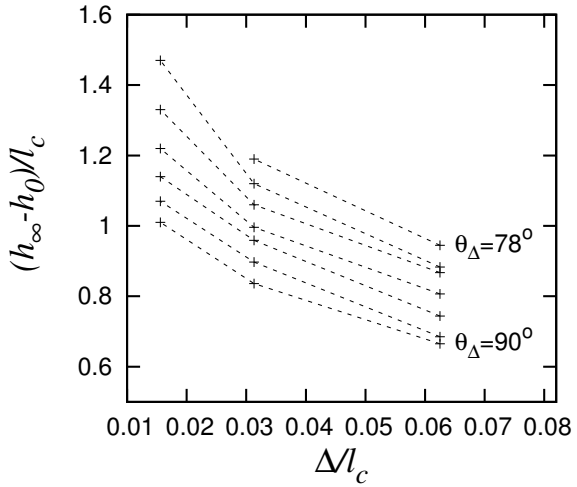

$\mathrm{Ca} = 0.04$

Both contact line height and Ca_{cr} depend on the mesh size!

Stationary meniscus, $\mathrm{Ca} = 0.043, \theta_\Delta = 90^\circ$

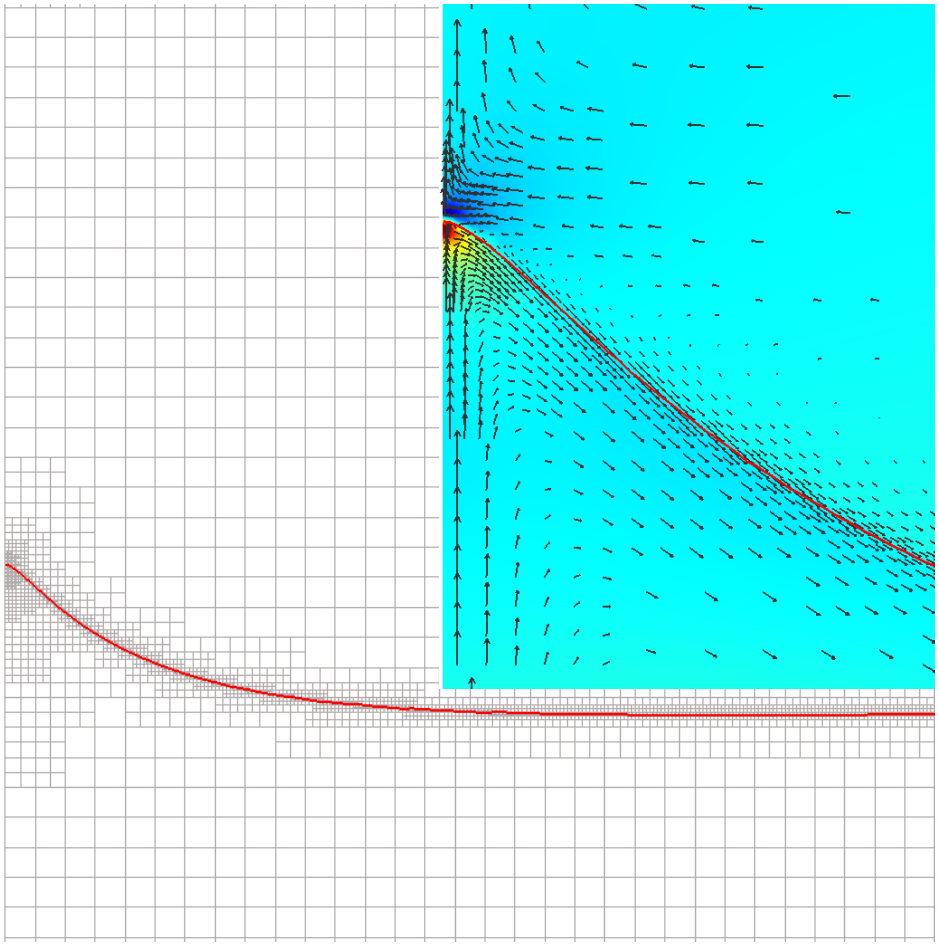

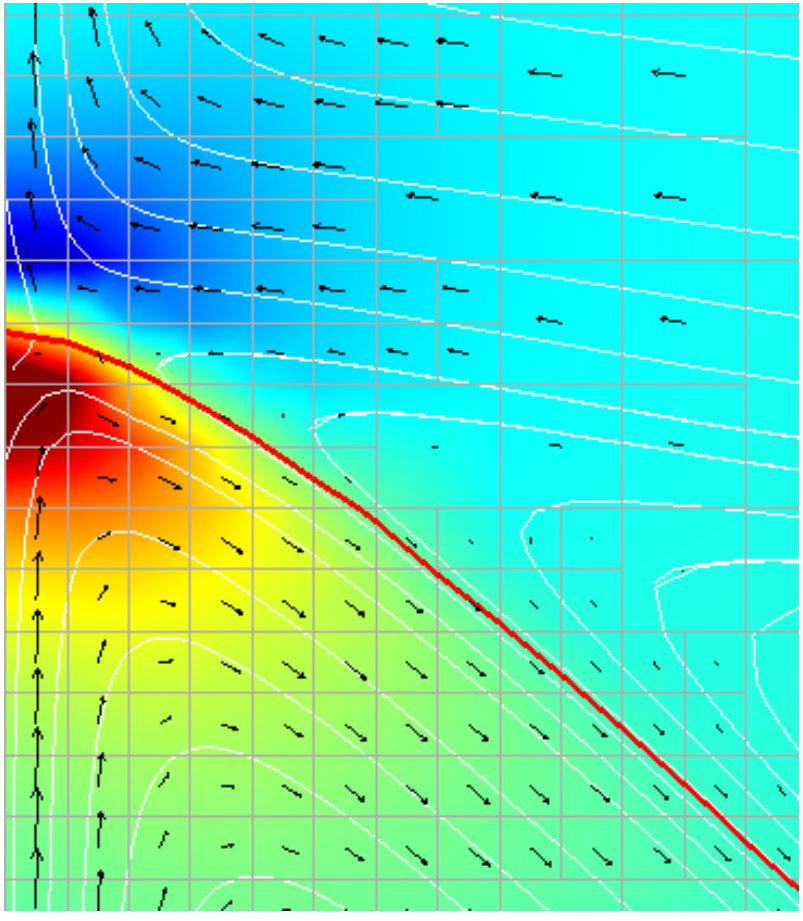

Transition to LLD film, $\mathrm{Ca} = 0.045, \theta_\Delta = 60^\circ$

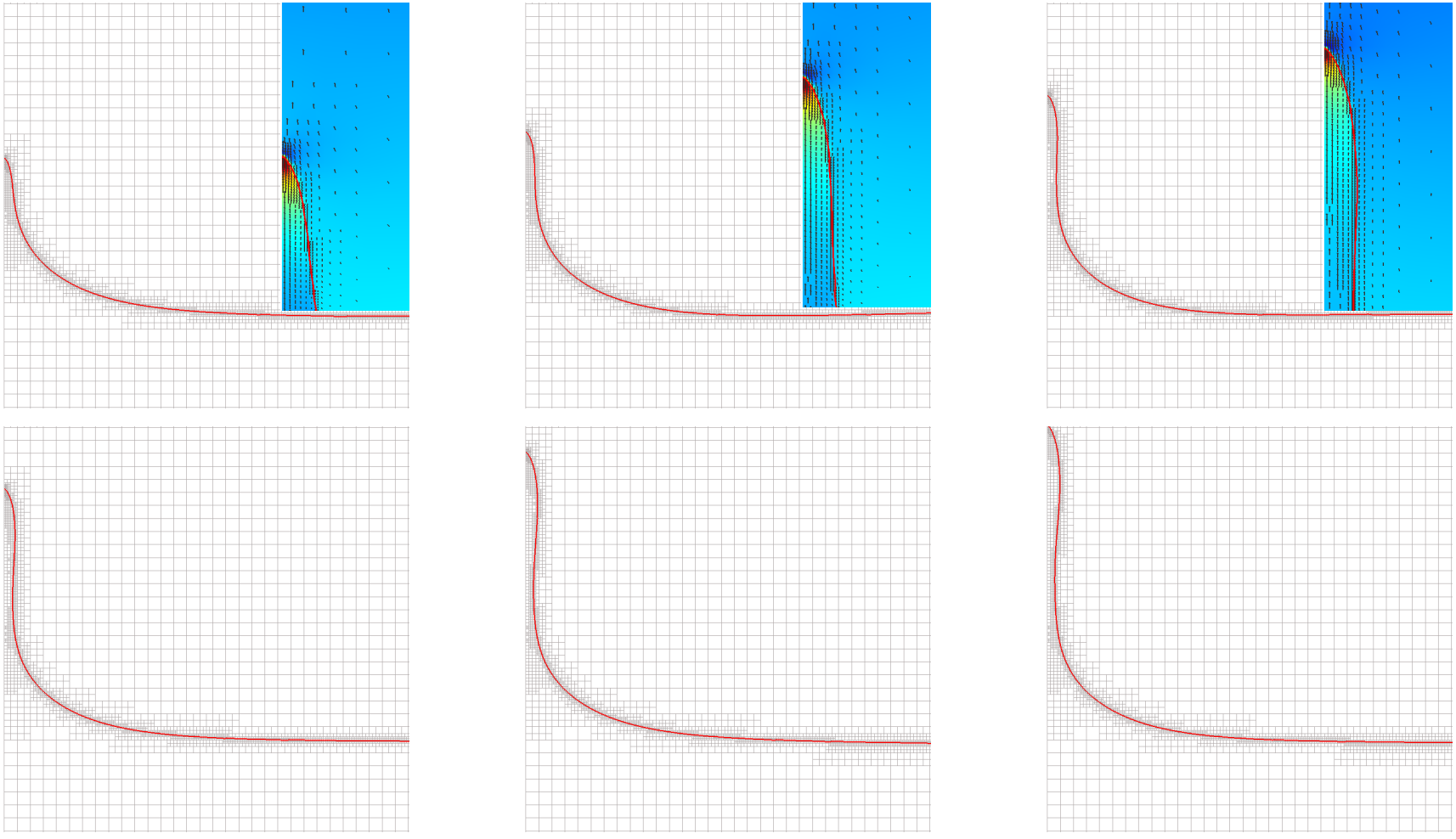

Asymptotic matching solution

R. G. Cox [JFM (1986)]:

$$G(\theta_{out}) = G(\theta_{in}) + \mathrm{Ca}\ln(\varepsilon^{-1}) + O(\mathrm{Ca})$$

$$G(\theta) = \int_0^{\theta} \frac{d\theta'}{f(\theta', q)},$$

$$f(\theta, q) =$$

$$\frac{2\sin\theta\{q^2(\theta^2 - \sin^2\theta) + 2q[\theta(\pi - \theta) + \sin^2\theta] + [(\pi - \theta)^2 - \sin^2\theta]\}}{q(\theta^2 - \sin^2\theta)[(\pi - \theta) + \cos\theta\sin\theta] + [(\pi - \theta)^2 - \sin^2\theta](\theta - \cos\theta\sin\theta)}$$

- As $\mathrm{Ca}, \varepsilon \to 0$, $\theta_{out} \to \theta_{in}$ if $\mathrm{Ca}\ln(\varepsilon^{-1}) \to 0$.
- $\varepsilon = r_m/r$ is not uniquely defined.
- Effect of corresponding small scales can be summarized with θ_{in} and the microscopic length scale r_m.

A numerical procedure

For each numerically imposed static contact angle θ_Δ and grid size Δ, we determine a critical Ca_{cr}.

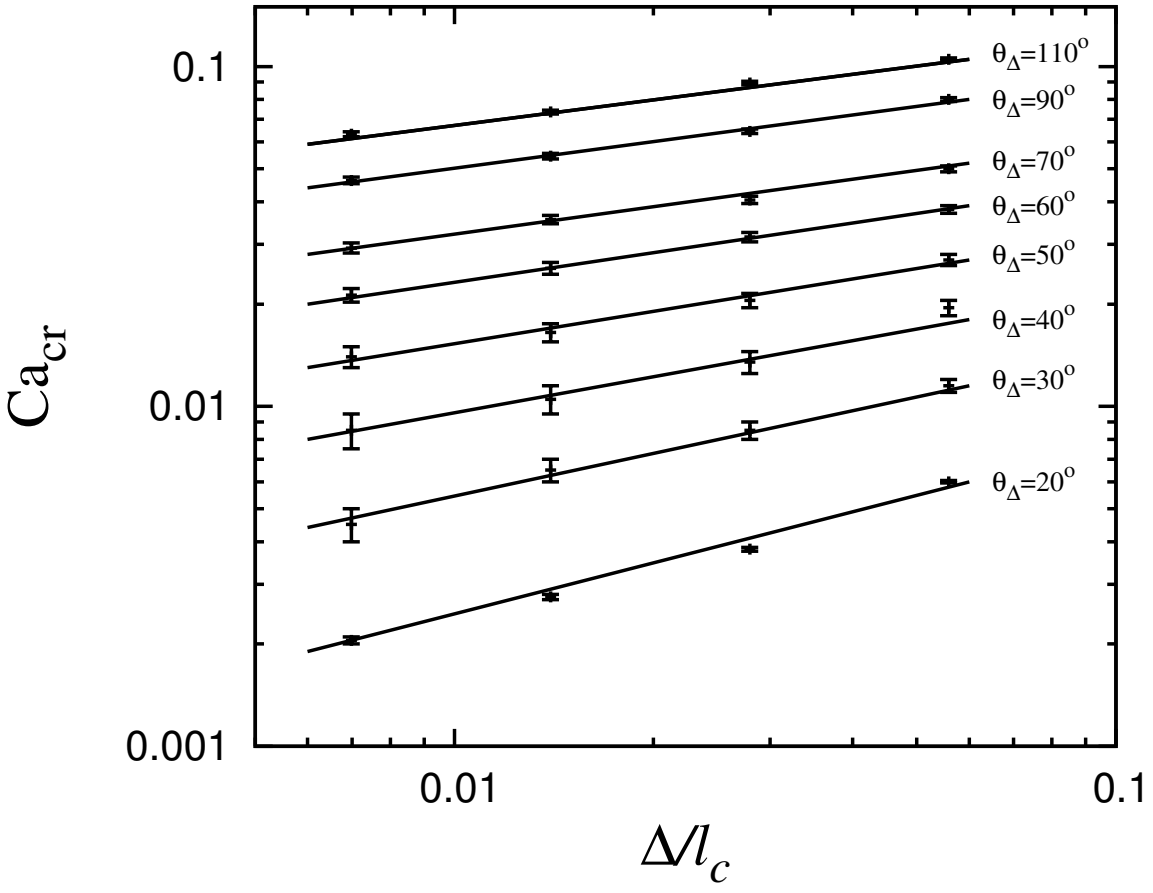

$$l_c = \sqrt{\gamma/[(\rho_1 - \rho_2)g]}$$

Results

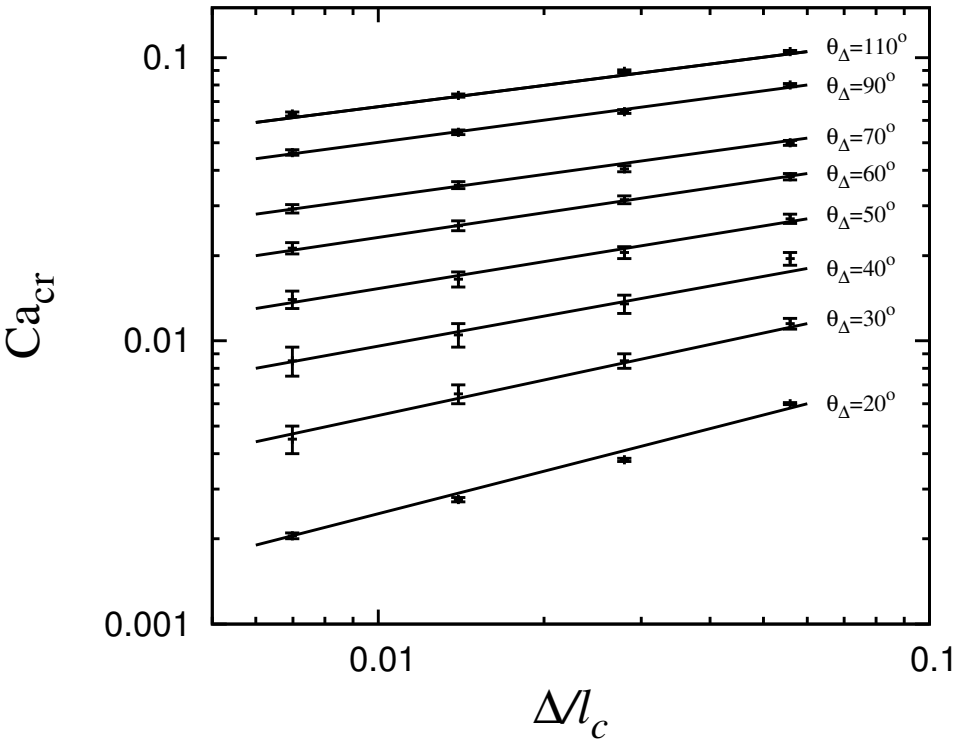

$$G(\theta_{out}) = G(\theta_{in}) + \mathrm{Ca}\,\ln(\varepsilon^{-1})$$

$$G(\theta_{in}) = \mathrm{Ca}_{cr}\,\ln(r/r_m)$$

$$\mathrm{Ca}_{cr} = (\theta_{in}^3/9)\left[\ln\left(\frac{[\mathrm{Ca}_{cr}]^{1/3}\theta_{in}}{18^{1/3}\pi[\mathrm{Ai}(S\mathrm{max})]^2\sqrt{2}\lambda}\right)\right]^{-1}$$

At the transition, $\theta_{out} \to 0$:

$$G(\theta_{in}) = \mathrm{Ca}_{cr} \ln(r/r_m)$$

$\theta_{in} \to 0$:

$$\mathrm{Ca}_{cr} = (\theta_{in}^3/9) \left[\ln \left(\frac{[\mathrm{Ca}_{cr}]^{1/3} \theta_{in}}{18^{1/3} \pi [\mathrm{Ai}(S\mathrm{max})]^2 \sqrt{2} \lambda} \right) \right]^{-1}$$

In the numerical model:

$$\theta_{in} \to \theta_\Delta, \quad r_m = \Delta/\phi(\theta_\Delta)$$

$$\mathrm{Ca}_{cr} = (\theta_\Delta^3/9) \left[\ln \left(\frac{[\mathrm{Ca}_{cr}]^{1/3} \phi(\theta_\Delta)}{18^{1/3} \pi [\mathrm{Ai}(S\mathrm{max})]^2 \sqrt{2} \Delta} \right) \right]^{-1}$$

Comparison with theoretical predictions

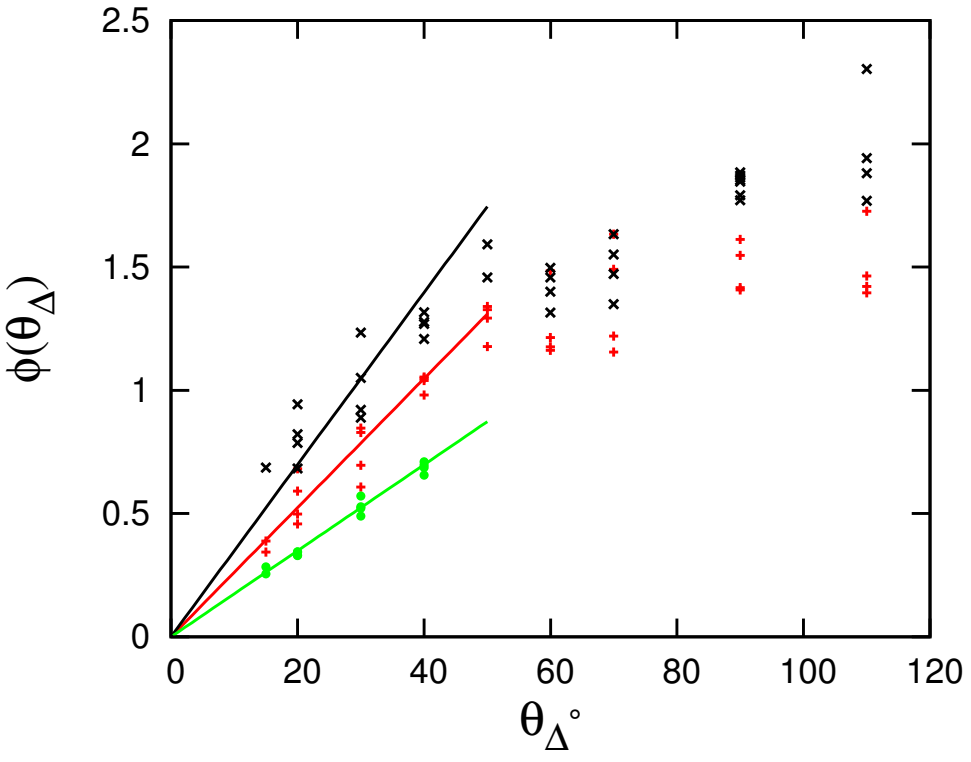

$$\phi(\theta_\Delta) = (18^{1/3}\pi[\mathrm{Ai}(S\mathrm{max})]^2\sqrt{2})\frac{\Delta}{\mathrm{Ca}_{cr}^{1/3}}\exp\left[\frac{\theta_\Delta^3/9}{\mathrm{Ca}_{cr}}\right]$$

$$\phi(\theta_\Delta) = \theta_\Delta, \quad \lambda \approx 0.6\Delta$$

Conclusions

- The results serve as an indirect verification of the Cox theory.
- Our numerical procedure can be thought of as a way to achieve mesh independent contact line simulations.
- Future work: extend the study to various scenarios, such as drop spreading, micro-layer formation, etc., to conform the universality of the numerical procedure.

Acknowledgments
J. Buongiorno and A. Guion (MIT)
S. Popinet and S. Zaleski (UPMC)
R. Scardovelli (Università di Bologna)
NSF DMS-1320037 and NSF-CBET-1604351